DEVELOPMENT AND CHARACTERIZATION OF BIOMIMETIC PEPTIDE-BASED BIOINK FOR DENTAL TISSUE ENGINEERING

A Thesis Submitted to
the Graduate School of Engineering and Sciences of
İzmir Institute of Technology
in Partial Fulfillment of the Requirements for the Degree of

MASTER OF SCIENCE

in Bioengineering

by
Zeynep ALTAN

March 2023
İZMİR

ACKNOWLEDGMENTS

Firstly, I would like to mention my deep and sincere gratitude to my supervisor Assoc. Prof. Dr. Ahu ARSLAN YILDIZ for her patience, help, counseling, and support throughout my thesis studies. I acknowledge TUBITAK 2210/C National MSc Scholarship Program in the Priority Fields in Science and Technology for financial support. I would like to thank Mutlu Devran YAMAN, a member of IYTE-MAM, for his contributions to the SEM and EDX parts of the thesis.

I am very grateful to my colleague and friend Özüm Yıldırım for her guidance, valuable friendship, encouragement, and deep support throughout my graduation life and personal life. I especially thank Biomimetics Research Group members; Ece ÖZMEN, Alper Baran SÖZMEN, Başak ÇOBAN, Necmettin Arda PİŞİRİCİ, Rümeysa BİLGİNER KARTAL, and Duygu ARSLANTAŞ for their friendship, support, help, and patience. I also want to express special thanks to my friend Sahranur TABAKOĞLU for her encouragement, and support.

Finally, I would like to show my deepest appreciation and love to my mother Berrin ALTAN for her endless encouragement and support.

ABSTRACT

DEVELOPMENT AND CHARACTERIZATION OF BIOMIMETIC PEPTIDE-BASED BIOINK FOR DENTAL TISSUE ENGINEERING

Recently, the role of molecular control in the tooth mineralization process has received much attention. Biomimetic scaffolds have been started to use in dental tissue engineering and regeneration due to their high applicability, biocompatibility, biodegradability, and mineralization capability. In this thesis, a hybrid biomimetic bio-ink; P11-4 peptide-based Quince Seed Hydrogel (QSH)/Gelatin (Gel) is used in 3D cell culture studies for dental tissue engineering applications. Pristine QSH, QSH/Gel, and P11-4/QSH/Gel bio-inks were characterized by FTIR and viscosity analysis, and their 3D bioprinting parameters were optimized. Hydrogels were crosslinked via 1-Ethyl-3-(3-dimethylaminopropyl) Carbodiimide (EDC)/N-Hydroxysuccinimide (NHS) coupling reaction and various hydrogel concentrations were investigated for scaffold fabrication. Characterization of produced scaffolds was performed by SEM imaging, mechanical testing, protein adsorption, and swelling analyses. As a result, the mechanical strength, viscosity, swelling properties, and surface characteristics of the biomaterial were evaluated. SaOS-2 human osteosarcoma cell line was used for 3D bioprinting studies. Cell viability analyses were performed via Live/Dead and MTT assays. Mineralization was investigated and assay was carried out with Alizarin Red Staining. According to obtained results, P11-4/QSH/Gel scaffolds provide high cell viability and proliferation rate compared to pristine QSH and QSH/Gel control groups. Also, with the addition of P11-4 to QSH/Gel, a certain amount of increase in mineralization was observed after day 7 on long-term cultured scaffolds. As a result of this study, it was concluded that P11-4-based QSH/Gel has a high potential to be used as a bio-ink in the production of 3D scaffolds for dental tissue engineering applications.

ÖZET

DİŞ DOKU MÜHENDİSLİĞİ İÇIN BİYOMİMETİK PEPTİT BAZLI BİYOMÜREKKEP GELİŞTİRİLMESİ VE KARAKTERİZASYONU

Son zamanlarda, diş mineralizasyon sürecinde moleküler kontrolün rolüne dikkat çekilmektedir. Biyomimetik yapı iskeleleri, yüksek uygulanabilirliği, biyouyumluluğu, biyobozunurluğu ve mineral oluşturma kabiliyeti nedeniyle diş doku mühendisliği ve rejenerasyonunda kullanılmaya başlanmıştır. Bu tezde, hibrit bir biyomimetik biyo-mürekkep; P11-4 peptit bazlı Ayva Çekirdeği Hidrojeli (QSH)/Jelatin (Gel), diş doku mühendisliği uygulamaları için 3-boyutlu hücre kültürü çalışmalarında kullanılmaktadır. Saf QSH, QSH/Gel ve P11-4/QSH/Gel biyo-mürekkepleri, FTIR ve viskozite analizi ile karakterize edilerek 3B biyobaskı parametreleri optimize edildi. Hidrojeller, 1-Etil-3-(3-dimetilaminopropil) Karbodiimid (EDC)/N-Hidroksisüksinimit (NHS) reaksiyonuyla çapraz bağlandı ve doku iskelesi üretimi için çeşitli hidrojel konsantrasyonları araştırıldı. Üretilen doku iskelelerinin karakterizasyonu, SEM görüntülemesi, mekanik test, protein adsorpsiyonu ve su tutma analizleri ile gerçekleştirildi. Sonuç olarak, biyomalzemenin mekanik mukavemeti, viskozitesi, şişme özellikleri ve yüzey özellikleri değerlendirildi. 3B biyobaskı çalışmaları için SaOS-2 insan osteosarkom hücre hattı kullanıldı. Canlı/Ölü ve MTT deneyleri aracılığıyla hücre canlılığı analizleri yapıldı. Hücresel ve hücre dışı bileşenler; DAPI, Aktin ve Kolajen Tip I immün boyamaları ile analiz edildi. Mineralizasyon araştırıldı ve Alizarin Red Staining ile mineralizasyon görüntülemesi yapıldı. Elde edilen sonuçlara göre P11-4/QSH/Gel doku iskeleleri, saf QSH ve QSH/Gel kontrol gruplarına göre yüksek hücre canlılığı ve çoğalma oranı sağlamıştır. Ayrıca, QSH/Gel'e P11-4 eklenmesiyle, uzun süreli hücre kültüründe 7. günden sonra mineralizasyonda belirli bir miktar artış gözlenmiştir. Bu çalışmanın sonucunda, P11-4/QSH/Gel'in dental doku mühendisliği uygulamaları için 3B yapı iskelelerinin üretiminde biyo-mürekkep olarak kullanılma potansiyelinin yüksek olduğu sonucuna varılmıştır.

TABLE OF CONTENTS

LIST OF FIGURES

Figure **Page**

Figure **Page**

Figure **Page**

LIST OF TABLE

Table **Page**

CHAPTER 1

INTRODUCTION

1.1. Scope of Thesis

This thesis aims to develop a novel biomimetic peptide-based bio-ink to fabricate 3-dimensional (3D) hydrogel scaffolds for dental tissue engineering applications. For this purpose, quince seed hydrogel (QSH) was used as a polysaccharide-based biopolymer to obtain bio-ink; Gelatin (Gel) was utilized as a pure collagenous protein like native ECM to improve cell adhesion and viability while providing a suitable microenvironment for cell adaptation. Therefore, Gelatin is a not printable polymer due to its poor mechanical properties and its viscosity depends on the temperature. QSH has excellent printability features and low cell viability on short-term cell culture experiments. Mixing of QSH/Gelatin provides us a natural polymer with good printability properties and high cell viability rates for long-term cell culture studies. In addition, P11-4 peptide was included in the bio-ink composition as a mineralization factor to mimic mineralized dental tissue.

1.2. Tissue Engineering

Tissue engineering is a multidisciplinary field that combines cell biology, biochemistry, medicine, and materials science (Eltom, Zhong, and Muhammad 2019). When tissues or organs are injured or they lose their function due to accidents or traumas, artificial organs or tissues are needed to reconstruct the damaged tissue or organs. These treatment procedures have been carried out by biomedical engineering until recently. Nevertheless, several challenges like biocompatibility and bio functionality could not be overcome with conventional approaches (Tappa and Jammalamadaka 2018). The problems that are faced during the utilization of artificial tissues or organs have started to be eliminated by an alternative approach which is called tissue engineering. Organ and tissue reconstruction with almost zero damage became possible with the emergence of this approach. One of the best advantages of

tissue engineering is the complete regeneration of the patient's own tissues and organs with high biocompatibility and functionality (Atala 1999).

Despite the abundancy of scaffold materials in use today, biomimetic scaffolds can aid and accelerate tissue regeneration, similar to the main tissue that represents the environment of cells in a living organism. Biologically inspired design or adaptation is called 'biomimetics' and it means mimicking living organisms or nature through the study of multi-disciplinary fields. This way, novel materials are produced, and chemical and biological processes are developed. As illustrated in Figure 1, the field of tissue engineering consists of three key components: cell sources, engineering materials, and tissue architecture. Owing to its customizable features, the tissue engineering area takes advantage of mimicking nature. Thus, tissue engineering has the potential to regenerate almost any organ or tissue. Biomimetic tissue engineering approaches aim to mimic the essential biological environment and process that plays role in restoring and healing diseased or damaged tissues through tissue remodelling. This multidisciplinary field achieves its goal by combining knowledge of cell biology, biochemistry, engineering, and molecular genetics (Bazos et al. 2011).

Cell, biocompatible scaffold, and growth factors are the three key points for tissue engineering applications. While the cell synthesizes new tissue matrices, the scaffold provides the appropriate environment for the effective regeneration of tissues. The function of growth factors and different additives is to support the cells to form new tissue, and the scaffold has the same properties as the natural extracellular matrix (ECM), which enables proliferation, differentiation, and biosynthesis of cells. Tissue engineering is a discipline that includes the construction of biodegradable artificial tissues *in vitro*. With this aim, it uses biological components and engineering principles for modification of cell growth and function implantation of complex structures consisting of suitable cells isolated from a specific target tissue, biologically active molecules that control the cell behaviour, and biocompatible scaffold materials (Berthiaume and Yarmush 2003). The ideal scaffold material should be biocompatible to improve cell attachment, proliferation, and viability. In addition, it should be biodegradable in time to allow tissue formation *in vivo*. Besides, scaffolds are used in three-dimensional (3D) cell culture to support the cells and provide their growth. Porosity is another property that scaffolds should possess, due to facilitates the transportation of oxygen, nutrient, and waste (Breslin and O'Driscoll 2013).

In tissue engineering, two different strategies, scaffold-based and scaffold-free, have been utilized for three-dimensional cell culture studies. In scaffold-free technique, a solid support like ECM or biomaterial is not necessary to form the 3D culture. Forced-floating, hanging drop, agitation, and magnetic levitation are the methods for scaffold-free 3D cell culture approach and they allow to create spheroids (Breslin and O'Driscoll 2013). On the other hand, the scaffold-based technique is based on the fabrication of a designed scaffold with desired features such as porosity, and biodegradability. After the fabrication process, cells are seeded on the scaffold (Young et al. 2002; Duailibi et al. 2004). Scaffolds can function as cellular and mechanical systems or delivery vehicles for cells in tissue regeneration, and the features of the used material must be sufficient to establish this. The required scaffold properties such as mechanical strength, porosity, degradation rate, and surface features depend on the target tissue that will be repaired (Roseti et al. 2017).

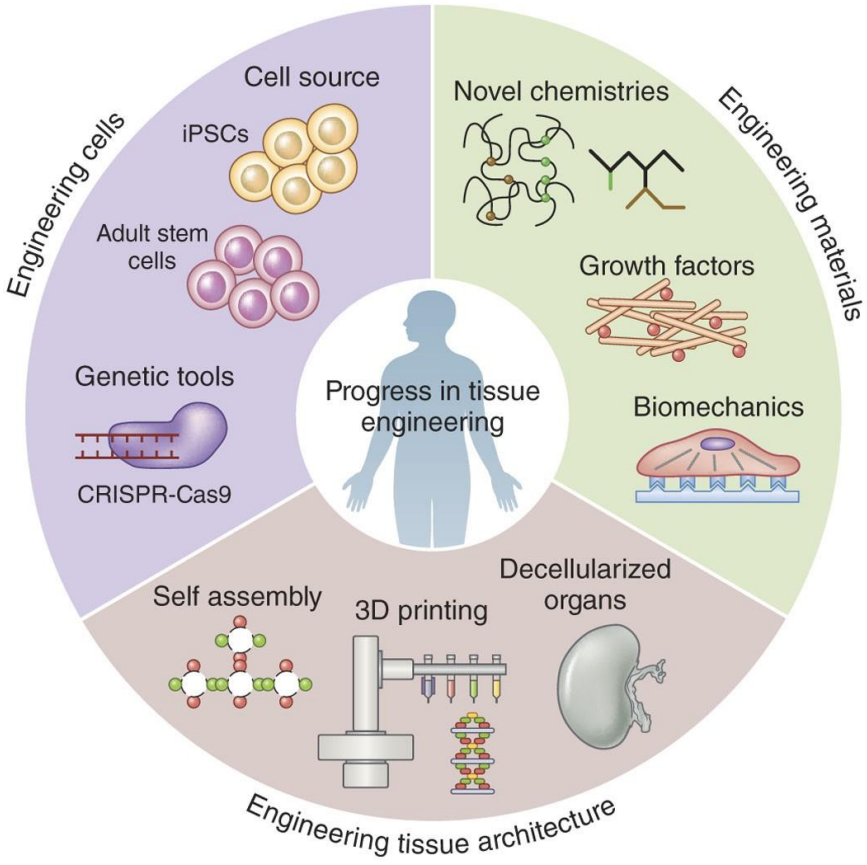

Figure 1. Three components of tissue engineering progress that are currently used. (Source: Khademhosseini and Langer 2016).

1.3. Extracellular Matrix

Extracellular matrix (ECM) is the three-dimensional (3D) non-cellular network consisting of water and extracellular macromolecules such as collagen, glycosaminoglycans (GAGs), enzymes, and hydroxyapatite ($Ca_{10}(PO_4)_6(OH)_2$) which provides a structurally stable skeleton for cells. It also contains growth factors for cell proliferation. The structure of ECM is a highly dynamic entity that is controlling the most important behaviours and characteristics of cells (Yue 2014). For these reasons, ECM has an important role in regeneration and repairing process of tissues (Fernandes et al. 2009; Ige, Umoru, and Aribo 2012).

In three-dimensional (3D) cell culture applications, cells in the environment have continuous interaction with the ECM, which regulates complex biological functions like cellular migration, apoptosis, regulation, and gene/protein expression. Therefore, in 3D cell culture, cell growth occurs in environments that closely mimic the structure and function of native tissue, and cell biology, drug screening, tissue engineering, and regenerative medicine are the important application areas of 3D cell culture (Langhans 2018). The scaffold materials must gradually degrade in the medium and be replaced by native ECM, allowing cells to secrete their own ECM during tissue formation. (Detsch et al. 2018).

1.4. Dental Tissue Engineering

Dental tissue engineering deals with problems caused by caries, trauma, and erosion, characterized by injury and loss of dental tissues or the entire tooth. Caries occurs when there is an imbalance between remineralization and demineralization in hard tooth tissue at the site of mineral loss. Therefore, common cavity treatment with drilling and filling the tooth involves repairing the injury, but not treating the disease itself (Alkilzy et al. 2018b). Although many advanced biomaterials are available for dental restoration, their utilizations are not fully satisfactory. In the last few decades, the role of molecular control on the tooth mineralization process and its cellular behaviour has received much attention. Injectable biomaterial scaffolds play a crucial role in dental tissue regeneration due to their high applicability in the dental field, especially when compared to preformed scaffolds. Many studies show that tissue engineering

approaches with the use of injectable biomaterials restore dental tissue and improve its biological purposes. (Haldar, Lahiri, and Roy 2019).

1.5. Dental Tissue Regeneration

Dental tissue is composed of a mineralized ECM which includes collagen type I. For the regeneration and mineralization of a tooth, cells with alkaline phosphatase activity and osteocalcin hormone are needed. A tooth has a bone-like structure, and the enamel part of the tooth is the hardest part of the body. Hydroxyapatite is the natural mineral form of calcium apatite in the dental microenvironment. The formation of hydroxyapatite crystals is obligatory for the mineralization process (Brown 2001). During odontogenesis, enamel formation is controlled by enamel matrix proteins, and these proteins are completely degraded at the end of maturation. As shown in Figure 2, dental tissue engineering can be summarized by designing and combining appropriate cells as well as materials and adding agents that promote tissue regeneration and cell proliferation to the system. Biomimetic approaches such as restoration of the tooth by using bio-inspired peptides, bioactive or natural biomaterials, and tissue engineering for remineralization have been recently used in restorative dentistry. Besides that, dental tissue engineering approaches have resulted in the regeneration and repair of lost or damaged dental tissues that can mimic their native structure and function (Sohail Zafar et al. n.d.).

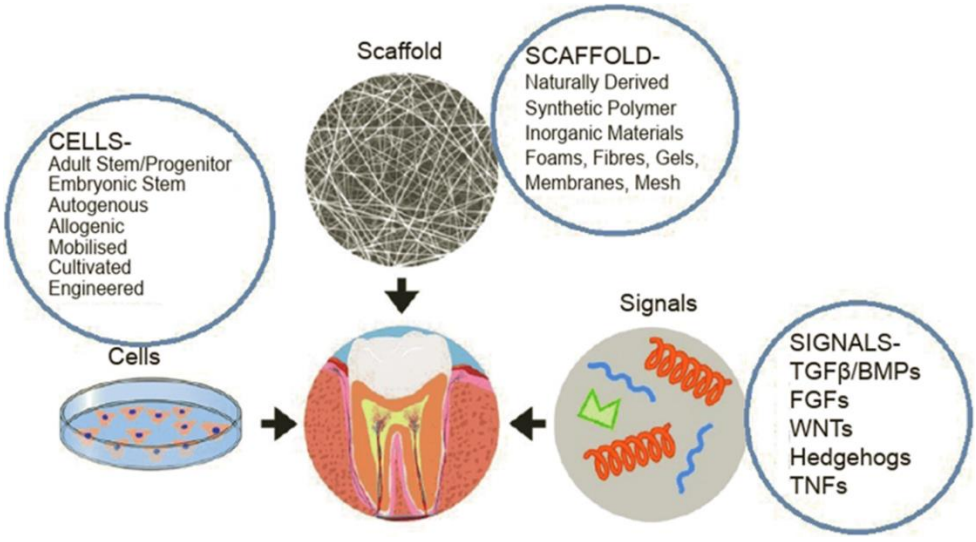

Figure 2. The key components for dental tissue engineering
(Source: Haldar, Lahiri, and Roy 2019).

1.6. Biomaterials for Scaffold Fabrication

Scaffold fabrication in tissue engineering applications begins with choosing the proper material for therapeutic purpose. Biologically based materials (biomaterials) are a specific class of materials designed and used to interact with biological systems for a purpose. They are categorized based on their origin as natural or synthetic, and according to degradability as biodegradable or non-biodegradable. They are used in biomedical applications as scaffold materials to improve, support, or regenerate damaged tissue or a biological function (Detsch et al. 2018). Two types of polymers can be used for the fabrication of scaffolds: synthetic and natural polymers.

1.6.1. Synthetic Polymers

Synthetic polymers are artificially produced in different types of reactions in laboratories (Shrivastava 2018). Many simple hydrocarbons can be transformed into polymers by polymerization reactions. Polycaprolactone (PCL) and Polyglycolic acid (PGA) are widely used examples of synthetic polymers.

PCL is a biodegradable polyester, and an important material due to its mechanical properties, low melting and glass transition point (Rani and Sharma 2021). It is highly compatible with other materials and convenient for the formation of polymers or co-polymers. Also, it can be prepared from renewable resources *via* chemical treatment of saccharides as bio-PCL (Flieger et al. 2003; Labet and Thielemans 2009). PCL is commonly used for modelling and as a raw material for ink for in 3D printing and importantly used in biomedical studies for bone and dental repair, drug release, and *in vivo* applications.

PGA is an essential biopolymer due to its good thermal and mechanical properties. PGA is highly biodegradable, which makes it favourable for medical applications. Production of PGA with higher molecular weight is important in order to increase mechanical stability for biomedical applications (Budak, Sogut, and Aydemir Sezer 2020).

PEG is a polyether compound derived from petroleum and widely used in medicine. It can be crosslinked and utilized as hydrogel by mimicking ECM for cell encapsulation and 3D cell culture studies (Zhu 2010). In addition, it is hydrophilic, it

has low toxicity and high solubility in water which are important advantages for tissue engineering applications (Manavitehrani et al. 2016).

1.6.2. Natural Polymers

Natural polymers have a great potential for increased cell viability and biocompatibility, and they are usually categorized as polysaccharides (such as cellulose and chitosan), proteins (collagen and fibrinogen) and polynucleotides (Schmidt and Baier 2000; Ige, Umoru, and Aribo 2012). Natural polymer-based hydrogels can be prepared using physical, chemical, or radiation cross-linking. While the physically cross-linked hydrogels exhibit poor mechanical strength, chemically cross-linked hydrogels have improved stability of the network structure. They also have a high ability to interact with cells by their hydrophilic properties (Rios et al. 2011).

Natural polymers are found in nature and can be extracted from plants, animals, and microorganisms. Since they are water-based and biocompatible, they are widely used in different areas such as pharmaceutical industry, medical imaging, and tissue engineering (ter Horst, Moiemen, and Grover 2019). Examples of naturally occurring polymers are silk, wool, nucleic acid, cellulose, and proteins (Shrivastava 2018). Their high biocompatibility, and water-holding capacity make them proper scaffold materials for tissue repair and regeneration purposes due to their similarity to ECM (ter Horst, Moiemen, and Grover 2019).

1.6.2.1. Hydrogels

Hydrogels can be explained as 3D crosslinked polymer networks. They are highly hydrophilic, and capable of swelling in water by keeping large volumes of fluid, and solutes within their swollen matrices. Hydrogels can be engineered to shrinking or expanding with the changes in environmental conditions (Ahmed 2015). Hydrogel-forming natural polymers include proteins such as Gelatin; and polysaccharides such as alginate. The usage of various functional biopolymers as scaffold materials in tissue engineering has accumulated a great potential. Hydrogels are commonly used to develop biocompatible scaffolds for tissue engineering studies as components of natural ECM (El-Sherbiny and Yacoub 2013a). They also have been utilized in drug-delivery

systems, biomedical production, and in different areas of biomedical engineering in the last few years (Kesharwani et al. 2021). They have been frequently used due to their high biocompatibility, and physical characteristics which allow permeability for O2, nutrients, and metabolites that are soluble in water. Collagen, hyaluronic acid, and chitosan are some of the polymers that have been used for hydrogel formation (Singh, Patel, and Singh 2016).

Natural polysaccharide-based hydrogels are widely used whereby their high biodegradability, biocompatibility, and bioactivity abilities. Depending on the cell, tissue, or biomaterial; sometimes natural hydrogels cannot achieve high cell proliferation or may degrade in the medium over time. Peptide-based hydrogels also play an active role as the molecular skeleton for target tissues and play an important role in normal metabolism, mimic the natural tissue microenvironment and respond to stimuli in the lesion environment. Amino acid structure of peptides provides various benefits to the cell culture process. Cells tend to attach protein parts of the scaffold and proliferate on them. Advantages of peptides give great application potential to polysaccharide-based hydrogels as biomedical materials (Zhu 2010).

Natural polysaccharide-based hydrogels are widely used whereby their high biodegradability, biocompatibility, and bioactivity abilities. Depending on the cell, tissue, or biomaterial; sometimes natural hydrogels cannot achieve high cell proliferation or may degrade in the medium over time. Peptide-based hydrogels also play an active role as the molecular skeleton for target tissues and play an important role in normal metabolism, mimic the natural tissue microenvironment and respond to stimuli in the lesion environment. Amino acid structure of peptides provides various benefits to the cell culture process. Cells tend to attach protein parts of the scaffold and proliferate on them. Advantages of peptides give great application potential to polysaccharide-based hydrogels as biomedical materials (Zhu 2010).

1.6.2.1.1. Quince Seed Hydrogel (QSH)

Quinces (Cydonia oblonga) are small trees with a good natural shape that is easy to maintain, with white or pink blossoms in spring and bears bright yellow fruits with a unique aroma. Quince fruit is native to Turkey and Iran (Ashraf et al. 2016), and it has antimicrobial and anti-ulcerative properties (Hamauzu et al. 2008; Jouki et al. 2013;

2014). In the middle of the fruit, there are brown seeds that are rich in phenolic compounds and flavonoids. In addition, the seeds have gelling properties due to their glucuronoxylan content. Quince seeds rapidly adsorb water and create hydrogel. The hydrogel obtained from quince seeds used in regenerative medicine for decades due to their antioxidative properties without any cytotoxic effect. Also, Quince seed is used in traditional medicine as a therapeutic biomacromolecule, widely used as an anti-inflammatory agent in wound healing (Izadyari Aghmiuni et al. 2020). Quince seed hydrogel (QSH) is a biomaterial based on glucuronic acid and xylose (glucuronoxylan). Glucuronoxylan is known as a widely available and easily accessible, biocompatible and water-soluble polysaccharide, which is highly swellable in water due to its important highly hydrophilic R-groups (such as amino, carboxylic acid, amide, and hydroxyl) (Izadyari Aghmiuni et al. 2020; Hemmati and Mohammadian 2009).

There are various studies in the literature on the use of QSH (Ghumman et al. 2022). Nevertheless, there are no studies on usage of a peptide-based bioprinted QSH as a dental bone tissue scaffold material. Therefore, in this thesis, the focus will be on the production and optimization of peptide-based hybrid QSH and pristine QSH scaffolds, and the mineralization process of these scaffolds in the future. The usage of peptide-based hybrid QSH scaffold as a 3D printable bio-ink for dental bone tissue engineering will be extensively investigated.

1.6.2.1.2. Gelatin-based Hydrogels

Gelatin is a natural biopolymer consisting of peptides and proteins which is obtained by the partial hydrolysis of collagen; it is the main structural protein of animal connective skin and bone tissues. Through its many advantages such as high-water uptake capacity, gelation ability, biodegradability, biocompatibility, texturing, thickening, and availability in the market, it has been considered as a high-potential candidate as a hydrogel component. Gelatin is widely utilized in the field of biomedical and tissue engineering applications. Gelatin solutions rapidly form hydrogels on cooling; but the materials have weak mechanical properties. The molecular weight and properties of Gelatin depend on the collagen source and extraction method, such as heat and enzymatic denaturation or extraction under alkaline conditions (Gelatin type B) or acidic treatment (Gelatin type A). It is readily available commercially and is more cost-

effective than collagen. Gelatin-based hydrogels are used in tissue engineering to promote cell adhesion and increase cell proliferation rate. In addition, they can be used for wound healing applications to their attractive fluid absorption properties. However, Gelatin-based materials are known for their poor mechanical properties, thermal instability, and short degradation times. These disadvantages can be mitigated by crosslinking the biomaterial from its free amine and hydroxyl groups as given in the Figure 4, such as the EDC/NHS coupling crosslinking methodology (Jaipan, Nguyen, and Narayan 2017; Agents 2021; Ghasemiyeh and Mohammadi-Samani 2019; Hoffman 2012).

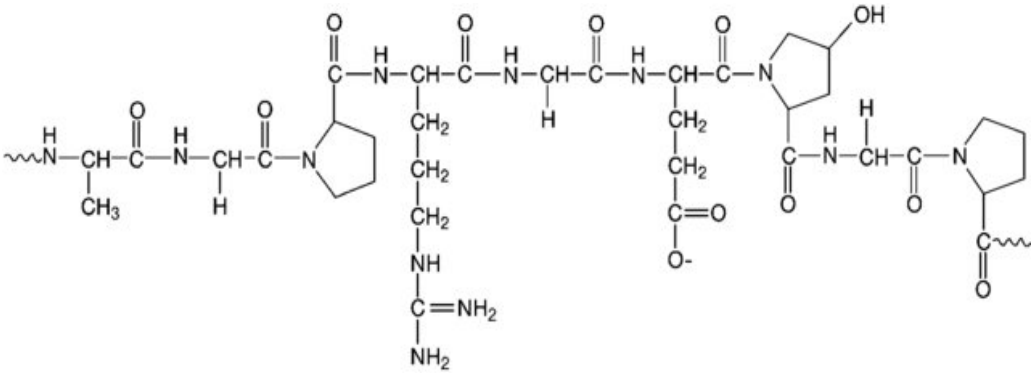

Figure 3. Basic chemical structure of Gelatin.

1.6.3. Additives for Mineralization

Enamel, dentin, and cementum are composed of both organic and inorganic natural components. The inorganic hard tissue parts of the teeth are composed of $Ca_{10}(PO_4)_6(OH)_2$, a biological apatite. Enamel is the part that has more inorganic content than dentin, bone, and cementum. Teeth are exposed to both acidic and basic food and beverage substances as ingredients of the oral microbiota; therefore, they have developed an unrivalled resistance and adapted to demineralization (Ahmed 2015). Biomineralization is a never ending process in which living organisms control the precipitation of inorganic crystals in organic matrices to form hybrid tissues such as enamel, dentin, cementum, and bone (Ahmed 2015). Understanding the mineral deposition process is important for developing remineralization treatments and regeneration as well as the development of dental tissue scaffolds.

Biological processes also include the formation of hard connective tissues where collagen fibrils form a scaffold for arrangement of calcium phosphate crystals (Cummins 2013). The use of peptides has been reported for various dental tissue regeneration applications including periodontal defects and bone regeneration (Bermúdez et al. 2021). As with calcium additives, with bio-inspired mineralization in peptide hydrogels, peptides can be used as a multifunctional template with the ability to provide a mineral source and structural controllability that facilitates hydrogel formation through self-assembly (Murai et al. 2021).

1.6.3.1. Natural Peptides

Natural peptides are found in all life forms. They are playing direct or indirect crucial roles in many physiological and biological processes. Natural peptides consist of short amino acid sequences and can be found free or encoded in proteins, therefore their release requires enzymatic hydrolysis (Hayashi, Ducancel, and Konno 2012; Daffre et al. 2008). Cell signalling aimed at translating and transmitting the biochemical message that triggers biological effects- is the primary function of peptides. In addition, many peptides can act as inhibitors in enzymatic processes. Peptides are a very promising bio-functional family of compounds owing to their functional roles in important processes, reduced size of the molecules, stability, and low immunogenic properties. These properties make them a promising element for diagnosis and treatment. Additionally, peptide-based scaffolds can easily be designed with modified biochemical, functional, or biophysical properties.

1.6.3.2. Synthetic Peptides

Synthetic peptides are chemically synthesized short polymer chains of amino acids. They can be used for various purposes, such as tissue engineering and regeneration applications. It is known that peptide-based structures have many advantages such as high chemical and biological diversity, potency and selectivity for their targets, low toxicity and good membrane penetration, and they can be used in different fields (Di Natale et al. 2020; Muttenthaler et al. 2021). Nevertheless, almost all peptides show poor stability in metabolism (La Manna et al. 2018). In the last few

years, synthetic self-assembly systems that can work as bioactive materials in biological environments have been used. Self-assembly of synthetic peptides has long been recognized as an excellent approach for the formation of desirable structures. Although the development of synthetic self-assembly peptides has often been inspired by principles observed in nature (for example, coupling of DNA and proteins) (Versluis, van Esch, and Eelkema 2016). Self-assembling β-sheet forming peptides form 3D fiber networks that support the tissue regeneration (Zhang 2017). Self-assembly peptides can be considered as a new class of agents capable of fabricating a range of micro/nanostructures that are highly attractive in the biomedical studies. By changing the amino acid composition of these peptides, it is possible to mimic several biological functions. When assembled into micro/nanostructures, they can be used for a variety of purposes, such as tissue regeneration, wound healing in regenerative medicine, and engineering. They have been used in a range of applications from surfactants to advanced materials (Zhang 2017; La Manna et al. 2021). Other significant advantages of these peptides include their biocompatibility and efficient targeting of molecular recognition sites (La Manna et al. 2021). By changing the amino acid compositions of these types of peptides, it is possible to mimic several biological functions.

1.6.3.2.1. P11-4 Peptide

P11- peptides are self-assembling, pH-triggered, and biocompatible synthetic peptides that are designed to use in biomaterials applications. The rationally designed synthetic P-11 peptide family consists of 11 amino acid peptides that self-assemble hierarchically into a B-sheet structure forming fibrils and fibers (Habibi et al. 2016). In particular, the P11-4 peptide shown in Figure 5 is used in dental tissue engineering due to its amino acid sequences. These peptides can form a 3D hydrogel and they have a high affinity to hydroxyapatite which is obligatory to form dental tissue. Regenerative medicine focuses on replacing damaged tissues with tissues similar to the native tissue. The P11-4 peptide has shown potential in the treatment by regenerating demineralized tooth tissue and preventing initial dental caries (Dawasaz et al. 2022b). P11-4 is designed to promote the formation of *de novo* hydroxyapatite crystals on its surface by increasing net mineral gain (Kind et al. 2017; Sedlakova Kondelova et al. 2020; Koch et al. 2019). No side effects, medical complications, or allergic reactions were reported

related to the treatments (Alkilzy et al. 2018a). The P11-4 peptide is designed to mimic enamel matrix proteins and to generate a 3D matrix that contributes to *de novo* hydroxyapatite formation, and it has been used for remineralization of subsurface lesions. (de Sousa et al. 2019; Dawasaz et al. 2022b). It interacts with collagen type I, increases the resistance of collagen fibers to proteolysis, and improves the stability (de Sousa et al. 2019). The Ca^{2+}-binding sites of the peptide surface correspond to the exact spacing of the Ca^{2+} ions in the hydroxyapatite crystal formation (Alkilzy et al. 2018a). The proper pre-positioning of Ca^{2+} ions decrease the activation energy of hydroxyapatite nucleation and increases the remineralization with formation of new hydroxyapatite crystals.

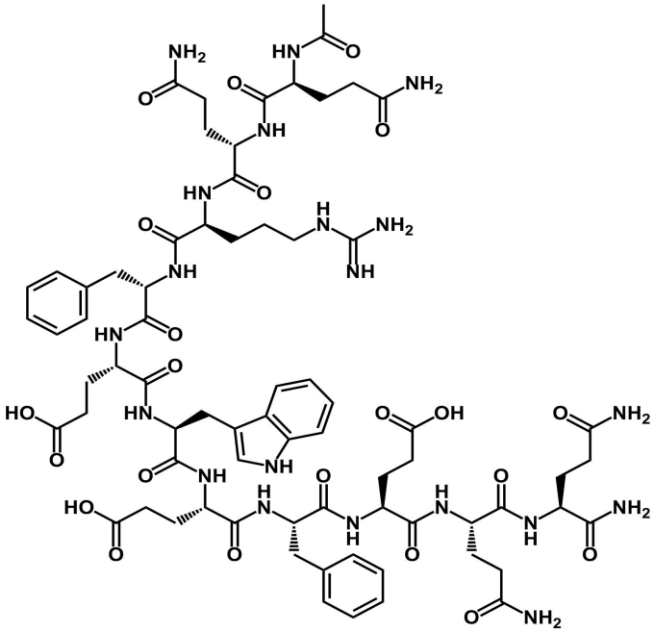

Figure 4. Molecular structure of oligopeptide P11-4.

1.7. Bioprinting

3D printing is an innovative manufacturing methodology of biomaterials, cells, and supporting components into complex 3D functional living tissues (Murphy and Atala 2014). 3D bioprinting plays an important role in producing 3D functional living structures that mimic natural tissues and organs. Various carbohydrate, protein, and nucleic acid-based biomaterials are used as biocompatible and biodegradable scaffolds that can support cell adhesion and proliferation in 3D printed tissues.

1.7.1. Bioprinting for Cell Culture Applications

Cell culture is the process of growing cells under controlled conditions outside their natural environment. A great deal of effort and prior knowledge is required to evolve cell culture into a system capable of reproducing in *in vivo* conditions. The ease of application of cell culture *in vitro* and limitations in animal models increases the dependence on this method.

Cell culture is conventionally carried out in a two-dimensional (2D) environment which includes adherent or suspended cells that can be grown on the surface of petri dishes or flasks depending on the type of cells. With the development of polymer technology, ECM applications have emerged in cell culture, which can now provide better growth conditions for adherent cells. Yet, this is not enough to provide a suitable microenvironment for living cells. Thus, the need for 3D cell culture arises. 3D cell culture polymer scaffolds that can be made from natural or biocompatible synthetic polymers and consist of cells growing on these scaffolds (Haldar, Lahiri, and Roy 2019). Scaffold-based 3D cell culture provides a supported growth better than the 2D culture. When engineering of the cell growth microenvironment is desired, 3D bioprinting provides great advantages and convenience to the application. It is possible with 3D bioprinting to carry out cell culture in 3D with an exactly designed and suitable environment that properly represents the microenvironment.

1.7.2. Bioprinting of Hydrogels

Advanced natural hydrogels have become popular in 3D cell culture platforms these days (Tibbitt and Anseth 2009). To provide specific requirements for scaffolds in tissue engineering applications, the physical properties of hydrogels, such as mechanical strength, can be engineered and controlled (El-Sherbiny and Yacoub 2013). There are certain properties, such as biocompatibility, and non-toxic degradability, that a hydrogel must have to be suitable for usage in tissue engineering applications.

To obtain the desired therapeutic results, scaffolds prepared from various biomaterials were used to contain sufficient cells to control cell functions (Nikolova and Chavali 2019). Hydrogels are usually prepared by hydrophilic polymer solutions and

converted into 3D network structures by chemical or physical crosslinking. In this way, 3D-structured hydrogels can encapsulate the cells and provide them with a proper ECM (El-Sherbiny and Yacoub 2013). Since the structure and physicochemical properties of hydrogels can be controlled by selecting different biomaterials and fabrication methods, they can provide the appropriate signalling environment for cells to function perfectly and tissue regeneration to occur (Özmen, Yıldırım, and Arslan-Yıldız 2023).

1.7.3. Biomimetic Mineralized Bioprinted Scaffolds

Mineralized biomaterials have been utilized to enhance dental tissue regeneration compared to their non-mineralized derivatives. Since non-mineralized scaffolds do not exhibit as good mechanical and surface properties as mineralized scaffolds, the usage of mineralized scaffolds provides promising methods for the development of functional biomimetic dental scaffolds. Especially, the mineralization on 3D scaffolds has become a promising approach for directed dental tissue regeneration (Wu et al. 2020). The mineralization term refers to the development of inorganic precipitation, such as calcium and phosphate ions, on an organic matrix. This process takes place throughout the life of the biological organism for the formation of bones, teeth, and homologous tissues. In substance, mineralization of dental tissue can be defined as the process of mineral deposition, in other words calcification, on the dental matrix for the development of new dental tissue. Human teeth consist of minerals containing 60-70% calcium phosphate ($Ca_3(PO_4)_2$) in the form of hydroxyapatite ($Ca_{10}(PO_4)_6(OH)_2$), and 20-40% collagen type I. During this mineralization process dental tissue forming cells, assist in the production of calcium phosphate crystals that then align in the collagen-based fibrous matrix (Dey 2020).

CHAPTER 2

MATERIAL AND METHODS

2.1. Materials

Axodual 3D-Bioprinter (AxolotlBio Systems) was used for bioprinting of scaffolds. Quince seeds were removed from quince fruits and the brown outer shell of the seeds was used for extraction. Gelatin Type A (BioShop) was used. 1-Ethyl-3-(3-dimethylaminopropyl) Carbodiimide (EDC), and N-Hydroxysuccinimide (NHS) were purchased from Sigma Aldrich and used as crosslinking agents. Bicinchoninic acid (BCA) kit was purchased from PierceTM, Thermo Scientific for protein adsorption assay. Cell culture experiments were performed by using Penicillin/Streptomycin (P/S), Trypsin-EDTA (sterile-filtered, 0.25%, BioReagent), high glucose Dulbecco's Modified Eagle's Medium (DMEM), Phosphate Buffered Saline (PBS, pH 7.4 10X); fetal bovine serum (FBS) from Gibco, and Dimethyl sulfoxide (DMSO) from AppliChem. SaOS-2 cell line (ATCC® HTB-85™) were used for bioprinting and mineralization studies. Rhodamine B dye from Merck and Fluorescein dye from Fluka Analytical were used for visualization of bioprinted scaffolds *via* fluorescence microscopy. P11-4 peptide obtained from Royobiotech company. Alizarin Red S (Alizarin Sulfonate Sodium) was purchased from Norateks. Propidium Iodide and CytoCalcein AM from (AAT Bioquest) were used for live/dead assay. Actin Cytoskeleton/Focal Adhesion Staining Kit from Sigma-Aldrich, and Anti-collagen Type-I from Merck Millipore were used for immunostaining assay.

2.2. Methods

The development and the production of biomimetic peptide-based QSH/Gel bio-ink for dental tissue engineering is illustrated in Figure 6.

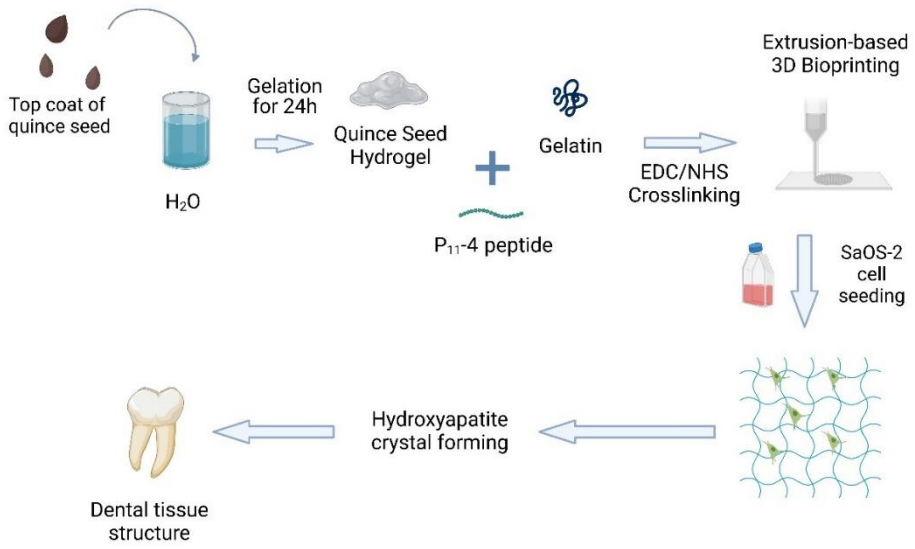

Figure 5. Schematic illustration of bio-ink production and utilization for dental tissue engineering (created in BioRender.com).

2.2.1. Extraction of QSH

Quince Seed Hydrogel (QSH) was prepared as described elsewhere (Guzelgulgen et al. 2021). Briefly, 100 mg/mL pristine QSH was prepared by mixing 500 mg brown outer shell of quince seeds with 5 mL ultrapure water. Gelation of QSH was completed after 24 hours of incubation at room temperature (RT). After the gelation is complete, pristine QSH was filtrated to remove seed residues (Figure 7).

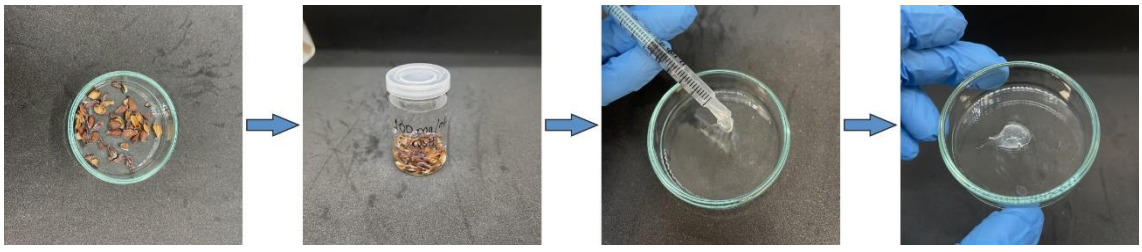

Figure 6. Depiction of preparation procedure steps of QSH.

2.2.2. Preparation of Bio-inks

75 and 100 mg/mL pristine QSH was prepared as described in section 2.2.1. After the gelation and filtration of QSH, EDC/NHS crosslinking method was used to obtain more durable bioprinted constructs. Crosslinking was done with a 5:1 (hydrogel: crosslinker) ratio and the mixture was homogenized for further use.

QSH/Gel hybrid hydrogel was prepared by mixing of 100 mg/mL pristine QSH, and 10 mg/mL Gelatin Type-A with a 10:1 (QSH: Gelatin) ratio. For the preparation of Gelatin, 10 mg Gelatin Type-A powder was weighed and mixed with 1 mL of UP H_2O for 30 minutes at 35ºC. QSH/Gel hydrogel mixture was mixed thoroughly and crosslinked with EDC/NHS with the above-mentioned ratio to fabricate more resistant bioprinted scaffolds.

P11-4 peptide was used for increasing the mineralization. Peptide-based QSH/Gel bio-inks were prepared by mixing P11-4 peptide solution with 100 mg/mL pristine QSH and 10 mg/mL Gelatin hydrogels. QSH/Gel hybrid hydrogel was prepared as described above. 1.59 mg P11-4 peptide was weighed and dissolved in 1 mL UP H_2O to prepare 600 μM stock peptide solution. For the preparation of P11-4/QSH/Gel hydrogel was prepared with 100 and 200 μM final P11-4 concentrations was added into the hybrid hydrogel mixture, respectively and the prepared solution was crosslinked by EDC/NHS. Bioprinting was performed immediately after preparing the bio-inks.

2.2.3. Bioprinting of QSH Bio-inks

Pristine QSH, QSH/Gel and P11-4/QSH/Gel bio-inks were printed *via* Axodual 3D-Bioprinter (Figure 8), SolidWorks was used to design G-code (Slic3r) based on STL files, and Repetier Host software was used for slicing and adjusting printing parameters. Printing parameters such as extrusion flux, moving speed, infill density, and structure models can be adjusted with G-code (Ouyang, Highley, et al. 2016). Bioprinting of pristine QSH and QSH/Gel hydrogels was performed by using a tapered smooth flow dispensing tip (nozzle) with a 25-gauge (0.437 mm) diameter on microscope slides to facilitate fluorescence microscopy visualization. The extrusion speed was adjusted to 10 mm/s for perimeter and infill printing. Single layer scaffolds with pre-designed square shapes (15 mm × 15 mm × 0.1 mm) (Figure 8) were printed using optimized

parameters. Hydrogel constructs were bioprinted with a height of 0.1 mm between each layer. In this study, a square model with grid pattern was used and infill density of constructs for printability analyses was chosen as 40% for each square of the grid to fit within the microscope viewing area, and 70% infill was preferred for cell culture studies. The flow rate of the dispensed bio-ink was controlled by adjusting the printing pressure between 3.0-5.5 psi, 4.5-8.0 psi, 8.5-13.0 psi, and 6.0-9.5 psi for 75 and 100 mg/mL pristine QSH, QSH/Gel, and P11-4/QSH/Gel, respectively.

Before 3D bioprinting, scaffold structure and printing parameters were adjusted in Repetier Host software. Later for the 3D bioprinting of pristine QSH, QSH/Gel, and P11-4/QSH/Gel constructs prepared bio-ink materials were mixed with EDC/NHS and loaded in a bioprinter syringe. Constructs were bioprinted by applying pressure in a range of 3.0-12.5 psi and bioprinted filaments were visualized *via* fluorescence microscope. Prior to cell culturing bioprinted constructs were swollen with UP H_2O, transferred into 24-well plate and UV sterilization was performed for 1 hour.

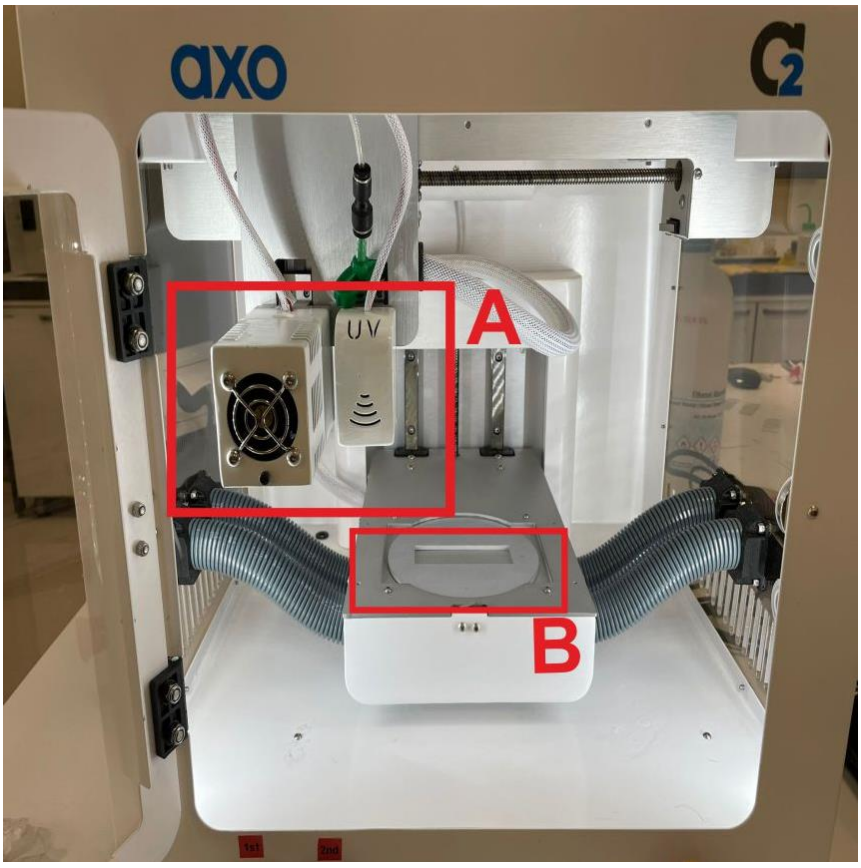

Figure 7. General view of 3D-bioprinter; (a) dual printhead system, (b) printbed.

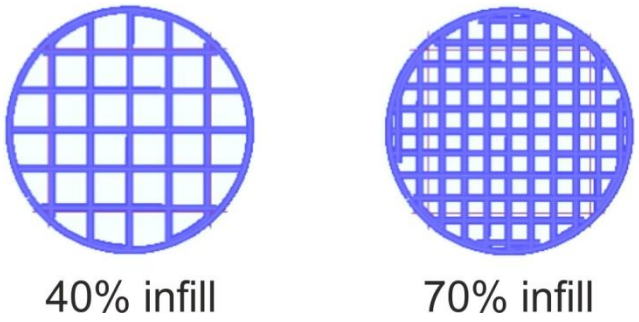

Figure 8. 3D scaffold models.

2.2.4. Characterization of Scaffolds

2.2.4.1. Printability Analysis

Printability analysis was performed by printing 75 and 100 mg/mL pristine QSH bio-inks, which was described in section 2.2.1. Additionally, 1 mM Fluorescein dye was added as 0.5% for the visualization by fluorescence microscope. Later visualization of filaments, pore and junction analysis was performed. ImageJ (NIH) image processing and OriginPro (Northampton, MA) data processing software were used to calculate and determine uniformity and pore factors.

Before bioprinting of constructs for 3D cell culture, printing parameters were optimized in terms of uniformity and pore factor analyses. Pristine QSH, QSH/Gelatin and P11-4/QSH/Gel bio-inks were prepared and loaded in a bioprinter syringe and their bioprinting was carried out using the parameters described in section 2.2.2.2. Filament and square models with grid infill were bioprinted by applying pressure in a range of 4.5-8.0 psi, 8.5-13 psi and 6.0-9.5 psi for pristine QSH, QSH/Gel, and P11-4/QSH/Gel, respectively. Bioprinted constructs were visualized by fluorescence microscope. Length of the bioprinted filament, perimeter and area of macropore structures were measured using ImageJ software, then uniformity and pore factor calculation was done using Equation 1 (Soltan et al. 2019) and Equation 2 (Ouyang, Yao, et al. 2016), respectively. Obtained data was plotted by OriginPro (Northampton, MA) software. Results represents the mean value of three individual data set for each parameter and formulation.

$$\text{Uniformity (U)} = \frac{Length\ of\ the\ practical\ line}{Length\ of\ the\ theoretical\ smooth\ line} \quad (1)$$

$$\text{Pore Factor } (P_R) = \frac{(Peripheral\ length)^2}{16 * Pore\ Area} \quad (2)$$

2.2.4.2. FTIR Analysis

FTIR analysis of hydrogels were obtained in 500-4000 cm^{-1} range using the UATR Two (PerkinElmer) Fourier Transform Infrared Spectroscopy in ATR mode to identify chemical content, crosslinking, and peptides.

2.2.4.3. SEM and EDX Analyzes

Energy Dispersive X-ray spectroscopy (EDX) is an analytical technique that is used for the chemical characterization/element analysis of materials. For the SEM analysis, both non-crosslinked and EDC/NHS crosslinked hydrogel samples were prepared as described in chapter 2.2.3. Prepared samples were freeze-dried and coated with a gold layer under Argon gas. SEM (FEI QUANTA, 250 FEG) was used for imaging process.

2.2.4.4. Viscosity Test

Viscosity measurements were performed with Thermo Scientific HAAKE Viscotester 550. 15 mL of pristine QSH and QSH/Gel were used for the viscosity test. Hydrogel samples were prepared using 100 mg/mL QSH and 10 mg/mL Gel. QSH/Gel hydrogel was prepared with 10:1 QSH: Gel ratio.

2.2.4.5. Mechanical Testing

Mechanical testing of bioprinted pristine QSH, and QSH/Gel were carried out with 100 mg/mL QSH and QSH/Gel (10:1). Mechanical testing of bioprinted structures was performed using the Texture Analyzer device (TA. XT Plus, Stable Micro Systems) with compression mode. A 5 kg load cell was used to perform the mechanical analysis.

Samples were prepared to have a diameter of 15 mm and a height of 3 mm. The compression test was carried out with a 35 mm diameter compression probe and the samples were compressed at a speed of 0.83 mm/s. A stress-strain graph was obtained, Young's Modulus and maximum strength were calculated using stress-strain graph.

2.2.4.6. Swelling Analysis

The water uptake capacities of pristine QSH, QSH/Gel, and P11-4/QSH/Gel constructs were analyzed using swelling analysis. The analysis assessed by comparing the wet and dry masses of bioprinted constructs before and after immersion in PBS. The dry weights (W_D) of the scaffolds were measured before soaking. Then scaffolds were immersed in PBS and incubated for varied time intervals (0.5, 1, 2, 3, 4, 5, 6, 8, 10, 12, and 24 hours). At determined time points, scaffolds were removed from the PBS, and weighed to determine the wet weight (W_W) values. The equilibrium swelling ratio (%) is calculated using Equation 3. (Begam, Nagpal, and Singhal 2003). (Milojević et al. 2021) Swelling test was performed using five replicates for each experimental group and results were given as mean values of percent swelling with standard deviation (SD).

$$\%\, Water\ Uptake = \frac{W_w - W_D}{W_w}\ x\ 100 \tag{3}$$

2.2.4.7. Protein Adsorption

The amount of adsorbed protein on pristine QSH, QSH/Gel, and P11-4/QSH/Gel scaffolds were determined using a total protein assay. Pristine QSH, QSH/Gel and P11-4/QSH/Gel were prepared in given concentrations and crosslinked in given ratio as described in section 2.2.1. Bovine serum albumin (BSA) stock protein solutions were prepared in PBS at varying concentrations (0, 25, 125, 250, 500, 750, 1000, 1500, 2000 µg/mL). The bioprinted constructs were immersed in prepared BSA solutions for 2 hours at 37°C and then they were rinsed 3 times with PBS solution. The initial samples and the final samples were collected from the supernatants before and after incubation. Adsorbed protein amount on constructs were determined using BCA Protein Assay Kit. Finally, absorbance was measured at 562 nm using a microplate spectrophotometer

(Fisher Scientific™accuSkan™GO UV/Vis) at RT. The calibration curve was plotted with the absorbance of the known BSA concentrations, and amount of adsorbed and solubilized proteins were quantified *via* obtained standard curve.

2.2.5. 2D Cell Culture and Maintenance

Human osteosarcoma cell line: SaOS-2 (ATCC® HTB-85™) was used for *in vitro* models. SaOS-2 cells were cultured in a complete growth medium containing 1% Penicillin-Streptomycin (P/S) and 10% Fetal Bovine Serum (FBS) in high glucose Dulbecco's Modified Eagle's Medium. Cells were cultured in a humidified incubator at 5% CO_2 and 37°C. The cells were subcultured about twice a week using Trypsin-EDTA solution when the cell confluency was reached to 80-90%.

2.2.6. 3D Cell Culture Studies

3D cell culture studies were carried out by seeding SaOS-2 cells on bioprinted pristine QSH, QSH/Gel, and P11-4/QSH/Gel scaffolds based on optimized parameters such as cell numbers, various hydrogel concentrations, and mixing ratio. The viability and proliferation of SaOS-2 cells were evaluated by Live/Dead and MTT analysis. Then, characterization of 3D cell culture was conducted by immunostaining of cellular/extracellular components, mineralization analysis by alizarin red staining, and morphological analysis by SEM.

2.2.6.1. Cell Viability Assays

Cell viability and proliferation analyses of injectable pristine QSH hydrogel and bioprinted QSHs were performed *via* Live/Dead and MTT assays.

2.2.6.1.1. Live/Dead Analysis

Live/Dead assay was done after SaOS-2 cells were seeded and cultured on bioprinted QSH scaffolds. 2D standard cell culture was used as a positive control group while bioprinted pristine QSH scaffolds were used as 3D control group. 0.1%

CytoCalcein AM and 0.1% Propidium Iodide in 10% complete medium was applied onto scaffolds and incubated for 30 minutes. After samples were analyzed *via* fluorescence microscope.

2.2.6.1.2. MTT Assay

Cell viability of SaOS-2 cells on bioprinted QSH scaffolds was assessed *via* MTT assay. 10% MTT assay solution was added into wells and incubated for 3 hours at 37$^{\circ C}$. After 3 hours, 400 µL DMSO for 3D samples and 200 µL DMSO for 2D samples was added to dissolve the formazan crystals and incubated on an orbital shaker at 37ºC for 30 minutes. The absorbance was measured at 565 and 650 nm using by UV/Vis spectroscopy.

2.2.6.1.3. Mineralization Analysis by Alizarin Red Staining

Alizarin Red Staining (ARS) was used to evaluate calcium phosphate-rich mineral deposits in 3D QSHs scaffolds. First of all after cell culturing, SaOS-2 cells on pristine QSH, QSH/Gel, and P11-4 based-QHS/Gel scaffolds were fixed for ARS staining (Gregory et al. 2004).

Mineralization assay was performed on SaOS-2 cells seeded on bioprinted pristine QSH, QSH/Gel, and P11-4/QSH/Gel constructs. They were incubated for 28 days, and separate samples were fixed in 4% PFA on day 1, 3, 5, 7, 9, 11, 13, 15, 21, and 28. Then, they were rinsed with UP H_2O. After the fixation step, 1% ARS solution was added onto fixed samples and incubated for 45 minutes at 25ºC. At the end of incubation, samples were rinsed 2 times with UP H_2O to remove excess ARS dye. Samples were analyzed *via* fluorescence microscopy.

2.2.6.1.4. Morphological Analysis

The morphology of SaOS-2 cells cultured on bioprinted pristine QSH, QSH/Gel, and P11-4-based QSG/Gel scaffolds were observed using SEM. For this purpose, cells were cultured on these scaffolds for 1, 7, 14, and 21 days, and then fixed using 2.5% Glutaraldehyde for 2 hours and 1% Osmium tetroxide for 1 hour. Then scaffolds were

rinsed with Ethanol (25%, 50%, 75%, 95%, and 100%). The visualization was performed using SEM (FEI Quanta, 250 FEG).

CHAPTER 3

RESULTS & DISCUSSIONS

3.1. Characterization of QSHs

Characterization of pristine QSH, QSH/Gel, and P11-4/QSH/Gel was performed by FTIR, SEM, mechanical testing, viscosity analysis.

3.1.1. FTIR Analysis

Fourier transform infrared (FTIR) spectroscopy was used to investigate the chemical composition of bio-inks and to determine the crosslinking efficiency by comparing the non-crosslinked and crosslinked pristine QSH (100 mg/mL), pristine Gel, QSH/Gel, pristine P11-4, and P11-4/QSH/Gel.

In this study, QSH derived from *Cydonia oblonga*, *Rosaceae* family; Gelatin Type-A, which was derived from porcine skin; and synthetically produced P11-4 peptide were investigated by FTIR and results are given in Figure 9.

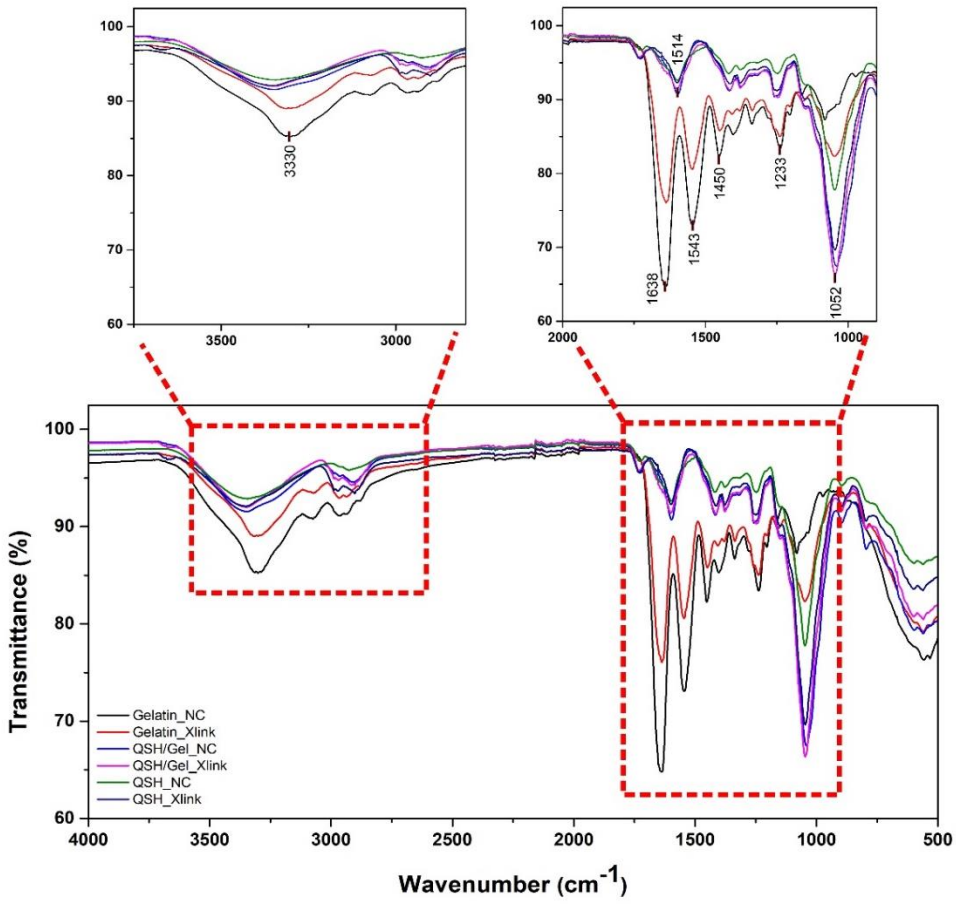

Figure 9. FTIR spectrum of non-crosslinked and EDC/NHS crosslinked *pristine* QSH, Gelatin and QSH/Gel bio-inks.

Table 1. Characteristic FTIR peaks observed after EDC-NHS crosslinking.

Bond type	**Wavenumber (cm^{-1})**
Amide A, N-H stretching	3370-3270
Amide 1, C=O stretching	1680-1630
Amide 2, N-H bending	1570-1515
Amide 3, C-N stretching	1260~

The characteristic peaks that were formed after EDC/NHS crosslinking are given in Table 1. According to Figure 9, QSH showed a characteristic peak at 3330 cm-1, which corresponds to the stretching of the hydroxyl (-OH) groups of glucuronic acid and xylose. The amide-I band observed between 1525 and 1502 cm-1 corresponds to N-H bending vibration as well as C-N stretching vibration in amide bonds. Also, the peak observed at 1638 cm-1 was consistent with C=O asymmetric and symmetric vibrations

of carboxylic acid (-COOH) groups of glucuronic acid, a content of QSH (Ghumman et al. 2022). The peak between 1205 and 980 cm-1 corresponds to the C-O-C groups (glycosidic linkage) of polysaccharides as QSH biomaterial. The peak observed at 1638 cm-1 corresponded to C=O asymmetric and symmetric vibrations of carboxylic acid (-COOH) groups of QSH.

EDC/NHS crosslinking occurs through the activation of carboxylic acid and amine groups to form stable NHS esters. EDC forms an amide bond, and the addition of NHS improves the binding efficiency and stability of amine-reactive intermediates (Figure 10). The shoulders between 1635 cm-1 and 1229 cm-1 correspond to the amide bonds formed after crosslinking. Characteristic peaks confirming the crosslinking were observed when non-crosslinked and crosslinked samples were compared as seen in Figure 9. Additionally, peaks around 3330 cm-1 corresponded to hydroxyl (-OH) groups of glucuronoxylan component in QSH and QSH/Gel were observed. Also, the intensity around 1233 cm-1 was increased, which is also confirming effective EDC/NHS crosslinking through amide bond formation.

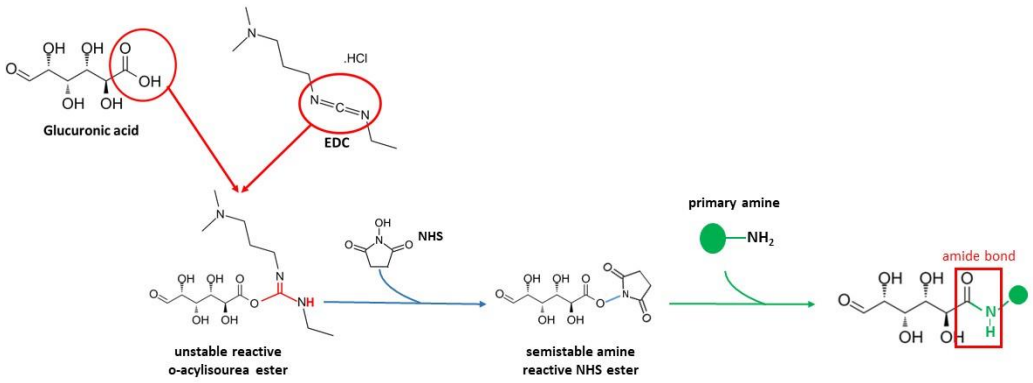

Figure 10. Crosslinking mechanism of EDC-NHS methodology.

After crosslinking of Gelatin or Gelatin containing bio-inks, it was confirmed that the Amide-I band corresponding to the C=O stretching vibration occurring at 1638 cm^{-1} and the amide-II band indicating the N–H bending vibration was seen at 1548 cm^{-1} in non-crosslinked Gelatin. Additionally, C–H bending vibrations were seen at 1416 cm-1, and the band at 1205 cm-1 indicated the C–N bond stretching vibrations of the amide III bond which is also proven by literature and given in Figure 9. (Shahin et al., 2022). The amide-III peaks in Gelatin were seen around 1240 cm^{-1}. The FTIR results of non-crosslinked and crosslinked QSH showed lower intensity for the C=O stretching,

and N-H bending compared to QSH/Gel samples. FTIR results of both crosslinked and non-crosslinked QSH and QSH/Gel samples showed characteristic peaks that confirm successful crosslinking.

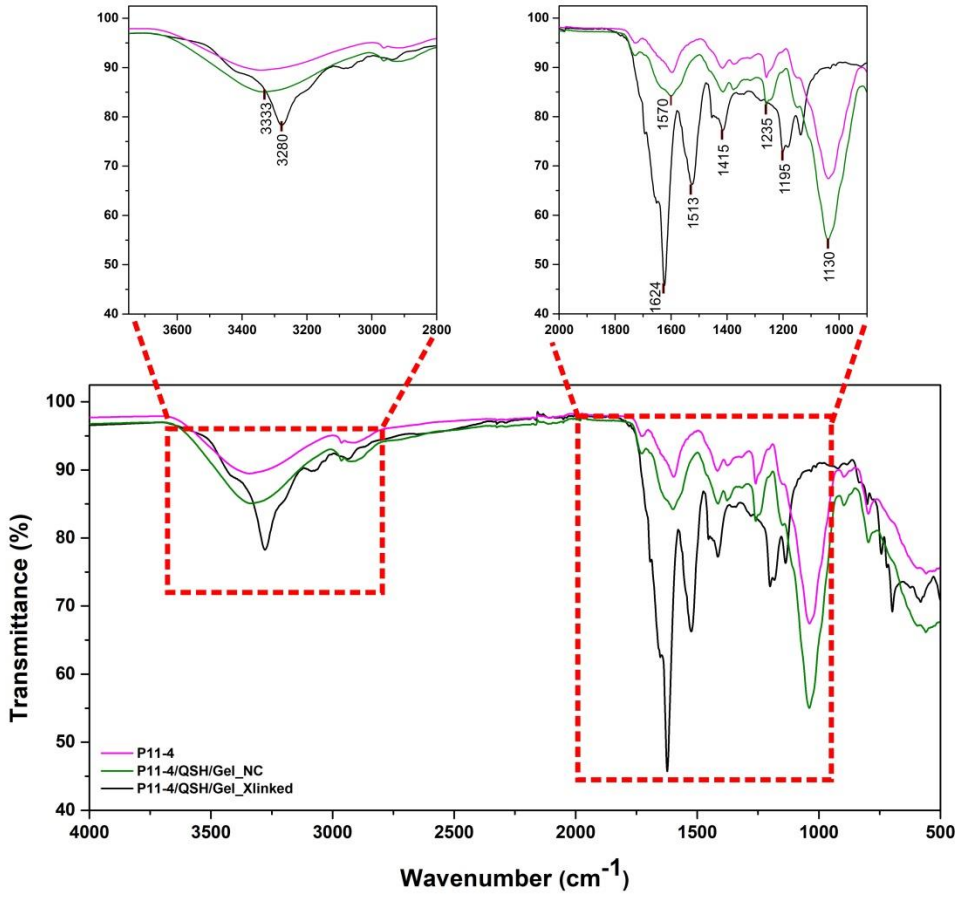

Figure 11. FTIR spectrum of P11-4 peptide and P11-4/QSH/Gel bio-inks.

After FTIR characterization of pristine QSH and QSH/Gel (Figure 9), the P11-4 peptide addition efficiency investigated by FTIR, and the results were given in Figure 11.

The Amide-I band, which occurs in the region 1600–1750 cm^{-1} is distinctive for proteins and inherently for peptides. The characteristic peaks between 1700 and 1576 cm^{-1} corresponded to C=O and C-N stretching and N-H bending of Amide-I and Amide-II bands. The band at 3200–3400 cm^{-1} indicates the presence of peptide bonds for the P11-4 peptide addition, which is supported by the literature (Rahali et al. 2017). Further, the peak at 1130 cm^{-1} shows the efficient EDC/NHS crosslinking of P11-4-based QSH/Gel when it is compared with pristine P11-4 peptide.

3.1.2. SEM Analyzes

SEM analysis was used to evaluate morphological features of pristine QSH, QSH/Gel and P11-4/QSH/Gel on micro scales.

Surface morphology of pristine QSH, QSH/Gel, and P11-4/QSH/Gel hydrogels were investigated by SEM imaging. As shown in Figure 12, all the three hydrogels have porous structures and there are interconnected porous to provide the proper spaces for cell adhesion and proliferation. Therefore, with suitable porous environment, highly porous P11-4/QSH/Gel can be used for dental tissue formation and mineralization.

EDX was used to evaluate the mineral composition of peptide-based bioprinted hydrogel scaffolds in the presence of SaOS-2 osteosarcoma cells. Cell cultured bioprinted QSH, QSH/Gel and peptide-based QSH/Gel scaffold samples were used for analysis. The content of calcium (Ca) and phosphorus (P) was analyzed by EDX. This analytical method provides a semi-quantitative simultaneous element analysis in dental tissue intended to be produced.

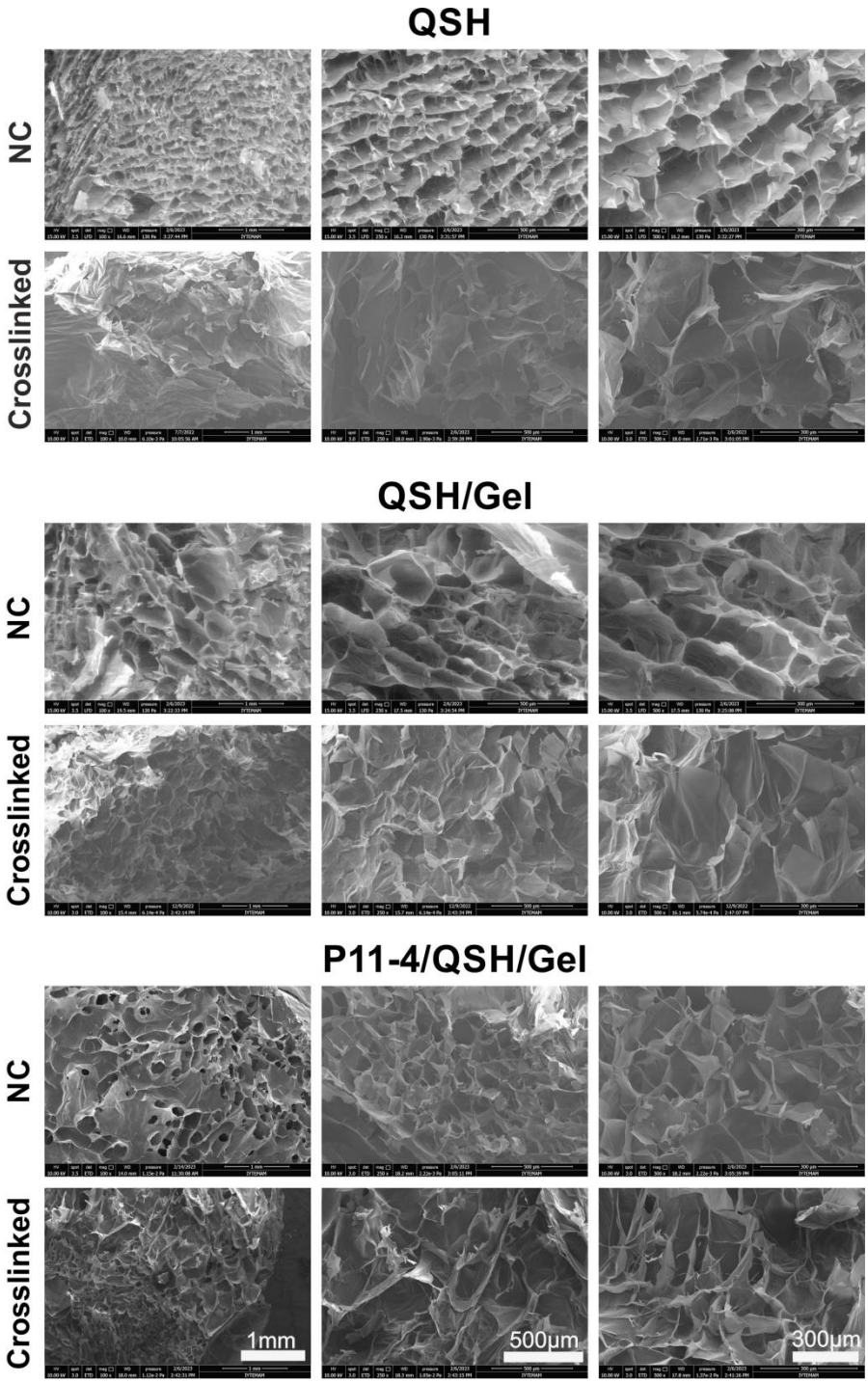

Figure 12. SEM images of the both non-crosslinked (NC) and crosslinked pristine QSH, QSH/Gel, and P11-4/ QHS/Gel hydrogels with varied magnifications.

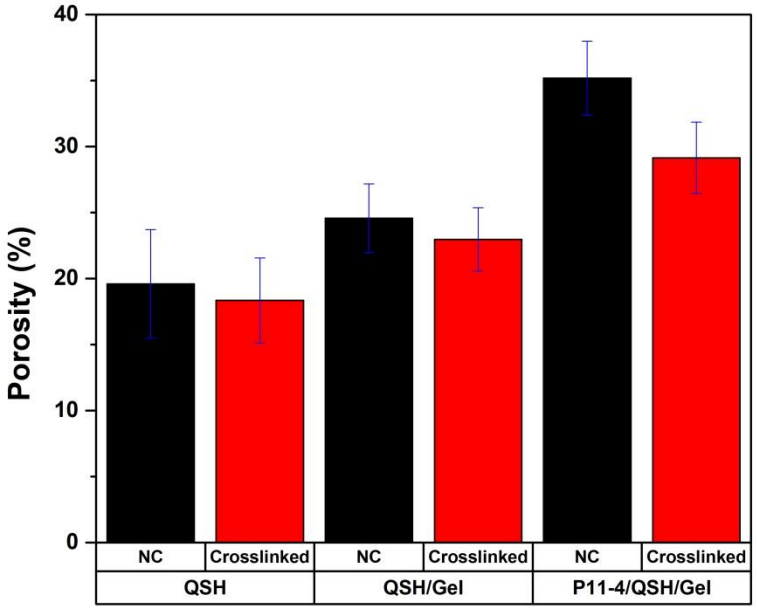

Figure 13. Porosity (%) for non-crosslinked (NC) and crosslinked pristine QSH, QSH/Gel, and P11-4/QSH/Gel hydrogels (scale bar: 500 μm).

According to the SEM images, porous structures were observed for all samples, and the % porosity of hydrogel samples was calculated by ImageJ software as given in Figure 13. The high percentage of porosity allows the cells to settle in these pores, increasing the rate of cell viability. In this study, considering that the viability of cells has an effect on increasing mineralization, a high pore percentage is aimed. When we compared the non-crosslinked and crosslinked samples, it can be said that adding the crosslinker slightly reduced the percent porosity of the hydrogels. Still, this amount is negligible considering the high impact of crosslinkers on mechanical strength. When the percent porosity ratios of the non-crosslinked samples were evaluated; the addition of Gel increased the porosity percentage by 4.61% compared to the pristine QSH, and the addition of P11-4 peptide increased the porosity percentage by 6.19% compared to the QSH/Gel. As a result, a significant increase in porosity was obtained by adding Gel and P11-4 peptide to QSH.

3.1.3. Mechanical Properties Test

The Young's modulus (*E*) was calculated by the linear region of compression plot. The results are given in Figure 14.

Average Young's modulus of pristine QSH, QSH/Gel, and P11-4 /QSH/Gel hydrogels were measured as 34.811, 63.379, and 78.015 respectively. According to the mechanical test results, the hardness of QSH was higher than that of the QSH/Gel and P11-4 /QSH/Gel hydrogels. Young's modulus, which shows how easily a material can stretch and deform under stress indicates that the QSH/Gel has lower strength compared to pristine QSH due to the poor mechanical stability of Gel. For the same reason, Young's modulus of P11-4 /QSH/Gel is lower than pristine QSH samples. P11-4 is a self-assembling peptide and consists of amino acids. Mechanical properties of peptides depend on peptide concentration, number of amino acids, and pH. In literature it is reported that the self-assembly peptide hydrogels showed poor mechanical properties (Raeburn, Cardoso, and Adams 2013), which confirms the low mechanical strength of P11-4 /QSH/Gel samples .

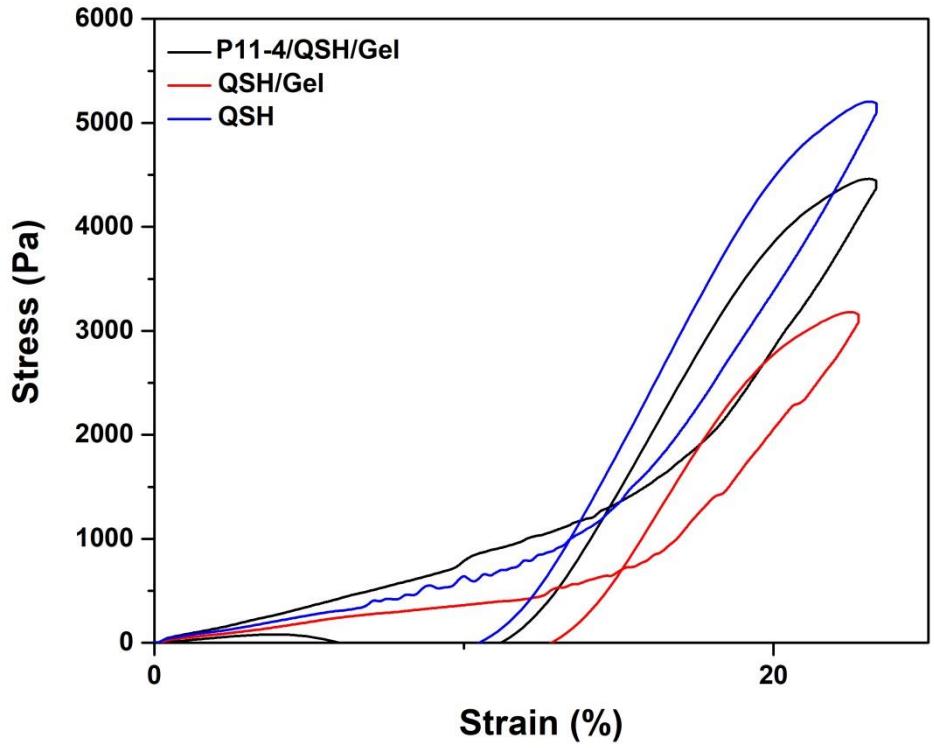

Figure 14. Stress–strain curve of crosslinked pristine QSH, QSH/Gel, and P11-4/QSH/Gel hydrogels.

3.1.4. Viscosity Test

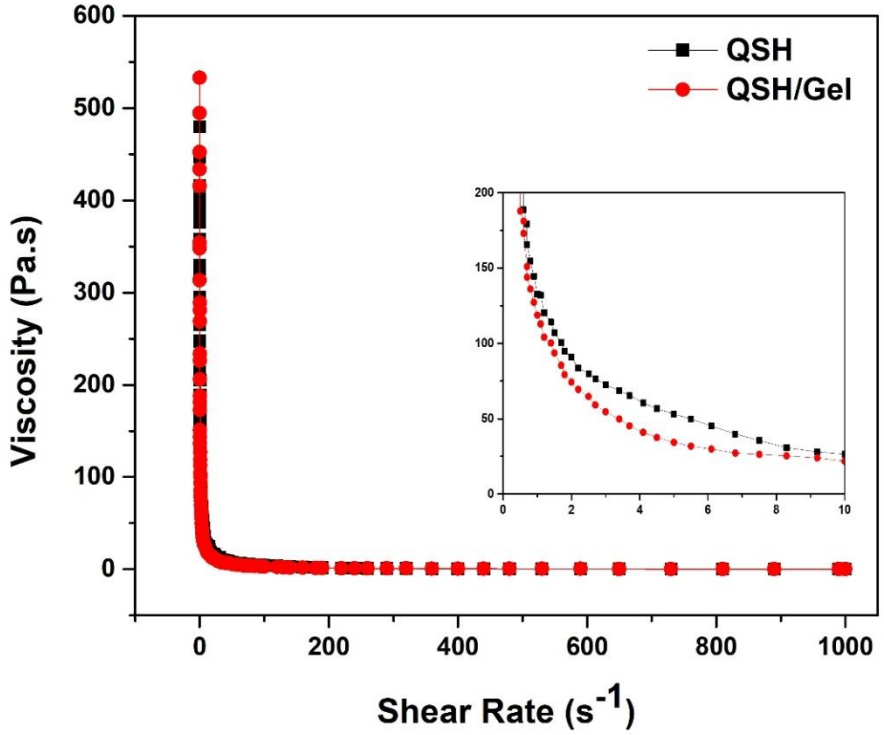

Figure 15. Rheological analysis of pristine QSH and QSH/Gel hydrogels against shear rate (s^{-1}) at 21°C.

Polymer solutions generally behave like non-Newtonian fluids, so viscosity depends on the shear rate at which it is measured. Both pristine QSH and Gel have shear-thinning properties (Garcia-Cruz et al. 2021), which means that their viscosity should be increased with an increase in shear rate. The increase of polymer concentration in a solution causes an increase in its viscosity. Pristine QSH is a glucuronoxylan-based biomaterial. Glucuronoxylan is a linear polymer that is linked by glycosidic linkage. Therefore, the glucuronoxylan content of hydrogel correlates with its viscosity. Also, the viscosity of Gelatin solutions increases with increasing Gelatin concentration and decreasing temperature. For this reason, the viscosity of pure Gelatin is difficult to control, however it can be adjusted by mixing it with QSH. The viscosities of pristine QSH and QSH/Gel were measured at shear rates between 0 and 1000 s^{-1} as plotted in Figure 15. As expected, the highest viscosity values were observed for pristine QSH, which decreased with increasing shear rate from 25-158 Pa·s, and the lowest viscosity value was seen for QSH/Gel between 55 to 24 Pa·s. Both QSH and QSH/Gel bio-inks comply with the power-law model. Coefficients of their consistency

for the power-law model were calculated using the viscosity vs shear rate. Results were obtained as 103,41 ± 3,57, and 57,66 ± 2,38 for 100 mg/mL QSH, and QSH/Gel (10:1) bio-inks, respectively. Results showed that a significant decrease in viscosity is obtained for QSH/Gel due to poor temperature dependent behaviour of Gel. Viscosity values were approximately 98 and 55 Pa·s for pristine QSH and QSH/Gel, respectively. These viscosity values are in a suitable range (3×10^{-2}–6×10^{4} Pa·s), and comparable to literature, especially for extrusion-based 3D bioprinting applications (Hospodiuk et al. 2017).

3.2. Optimization of QSH Scaffold Fabrication via Bioprinting

Bioprinting methodology was used to fabricate QSH scaffolds, and before cell culture studies and 3D construct fabrication, optimization of bioprinting parameters was performed by printability analysis.

3.2.1. Printability Analysis

Evaluating printability and shape accuracy is a crucial step for the development of a bio-ink. Printability analysis was performed in term of in pore factor and uniformity to compare the bio-inks.

3.2.1.1. Printing optimizations of QSH scaffolds

Optimization of bioprinting parameters for 75 mg/mL and 100 mg/mL pristine QSH bio-inks were carried out using filament (line) model for varied pressures ranging between 3.0-5.5 psi and 4.5-8.0 psi, respectively with 25G dispensing tip (Figure 16, Figure 17).

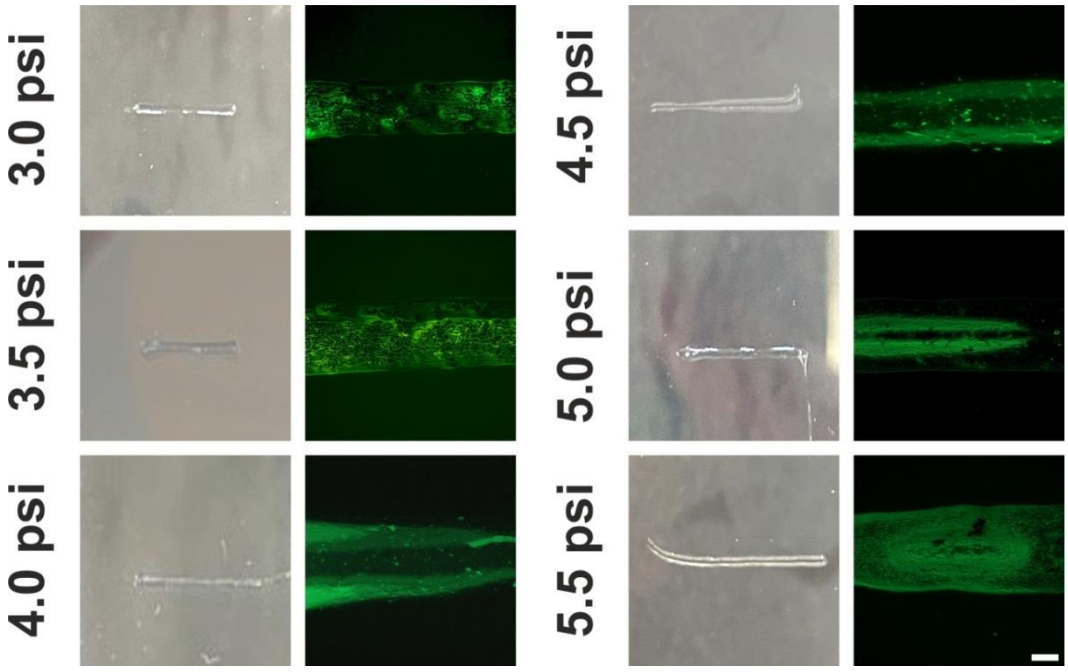

Figure 16. Bioprinting of 75 mg/mL pristine QSH bio-ink using 25G tip between 3.0-5.5 psi pressure values (scale bar: 200 μm).

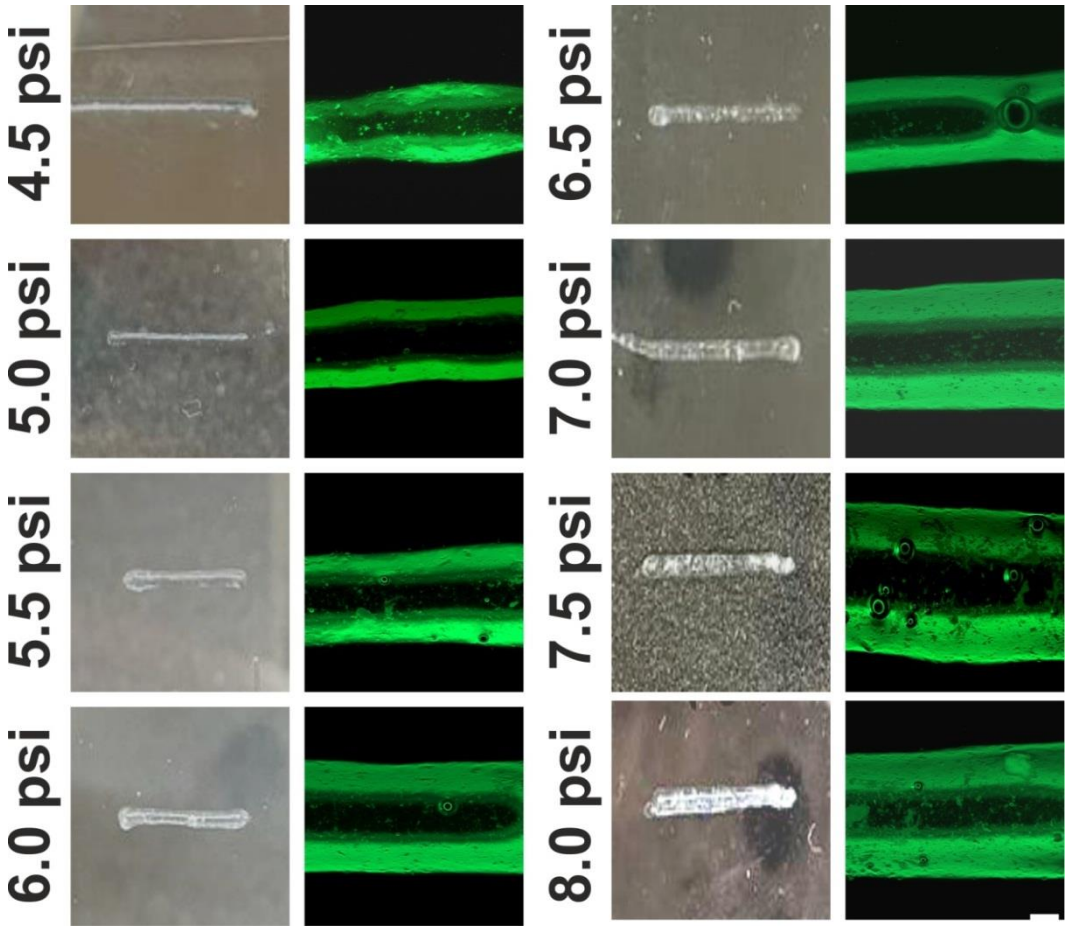

Figure 17. Bioprinting of 100 mg/mL pristine QSH bio-ink using 25G tip between 4.5-8.0 psi pressure values (scale bar: 200 μm).

Bioprinting of 75 mg/mL pristine QSH bio-ink resulted in regular filaments between 3.5-5.0 psi, and above 5.0 psi, the filament became thicker and irregular (Figure 16). Bioprinting of 100 mg/mL pristine QSH bio-ink resulted in regular filaments between 5.0-7.0 psi, and above 7.0 psi, the filament became thicker and irregular (Figure 17). By using these data uniformity values of 75 and 100 mg/mL pristine QSH bio-inks were calculated using Equation 1 and results are given in Figure 18.

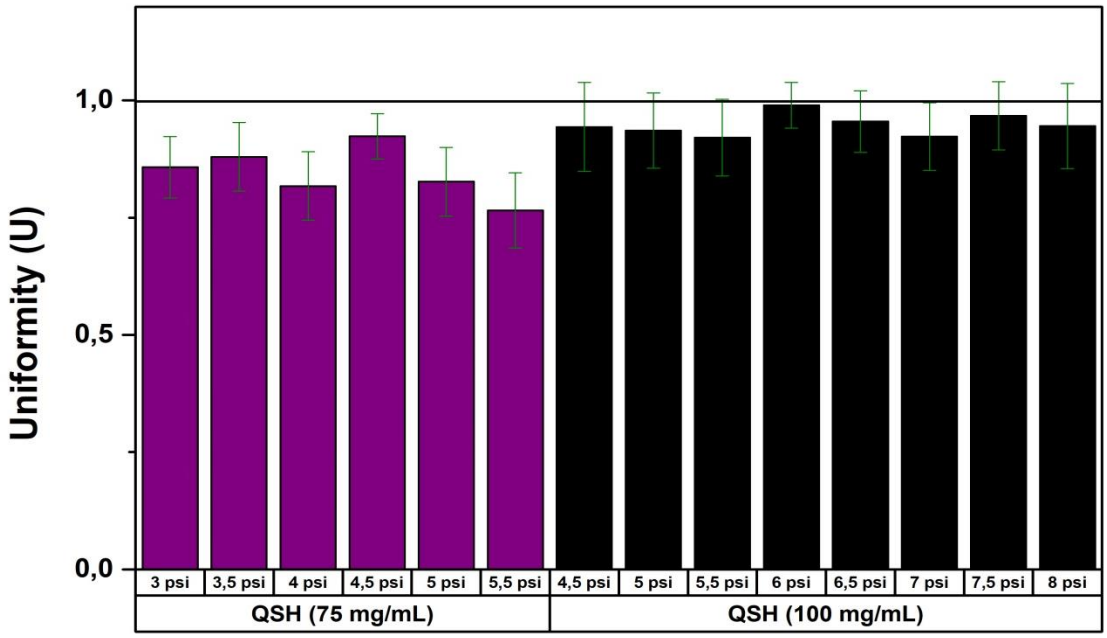

Figure 18. Uniformity analysis of 75 and 100 mg/mL pristine QSH bio-inks for 3.0- 5.5 and 4.5- 8 psi pressure values, respectively.

When the perimeter of a linear model is measured and normalized by the length of a perfectly straight line, it gives uniformity to a given bioprinted filament. 1.0 represents the maximum uniformity, and the diverged values indicate less uniform lines (Gao et al. 2018). According to Figure 18, the uniformity value of 75 mg/mL pristine QSH was closer to 1 at 4.5 psi, and for 100 mg/mL pristine QSH it was closer to 1 at 6.0 psi. uniformity values of 75 mg/mL QSH are unstable between pressures and far from the value of 1. Besides, pressure values are more stable and closer to 1 for 100 mg/mL QSH bio-ink. Considering these results, 100 mg/mL pristine QSH bio-ink is a more proper concentration than 75 mg/mL pristine QSH in terms of uniformity.

For the optimization of bioprinting parameters, a square grid scaffold model was also designed in SolidWorks software and used for bioprinting. Pore regulation of

scaffolds was optimized for 75 and 100 mg/mL pristine QSH bio-inks by 25G dispensing tip for varied pressure values between 3.0-5.5 psi and 4.5-8.0 psi, respectively. Photos and fluorescence microscopy images of 75 and 100 mg/mL pristine QSH bio-inks are shown in Figure 19, and Figure 20, respectively.

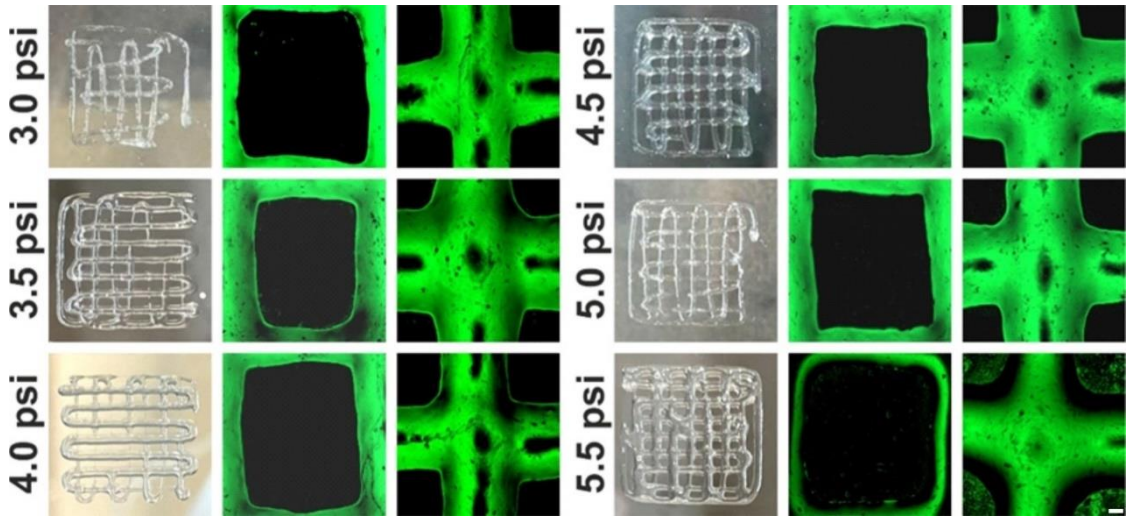

Figure 19. Bioprinting of 75 mg/mL pristine QSH bio-ink as square grid model using 25G tip for 3.0 -5.5 psi pressure range (scale bar: 200 μm).

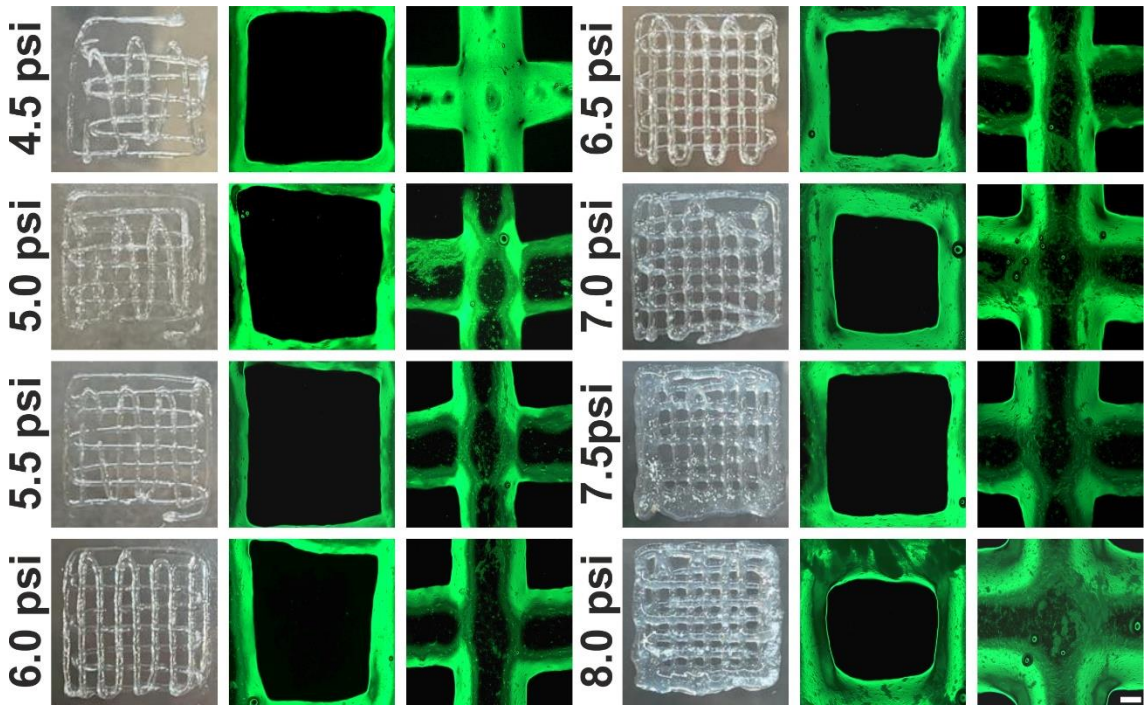

Figure 20. Bioprinting of 100 mg/mL pristine QSH bio-ink as square grid model using 25G tip for 4.5 and 8.0 psi pressure range (scale bar: 200 μm).

Bioprinted square grid models of 75 mg/mL pristine QSH bio-ink resulted in more regular pores above 4.0 psi while it was uniformly bioprinted between 5.0-5.5 psi (Figure 19). With 100 mg/mL pristine QSH bio-ink more regular shapes were produced after 5.5 psi, and it was uniformly bioprinted between 5.5. and 7.5 psi (Figure 20). In a study of our group, 100 mg/mL QSH was uniformly bioprinted between 6.8 and 7.2 psi with Axolotl 3D bioprinter (Yildirim and Arslan-Yildiz 2022). Due to the natural composition of biomaterials, gelation ability can change from batch to batch. It can be said that optimized parameters are close to each other and showed similarity for bioprinting studies. From onwards, pore factor values of 75 and 100 mg/mL pristine QSH bio-inks were calculated using these results and Equation 2, and results are given in Figure 21.

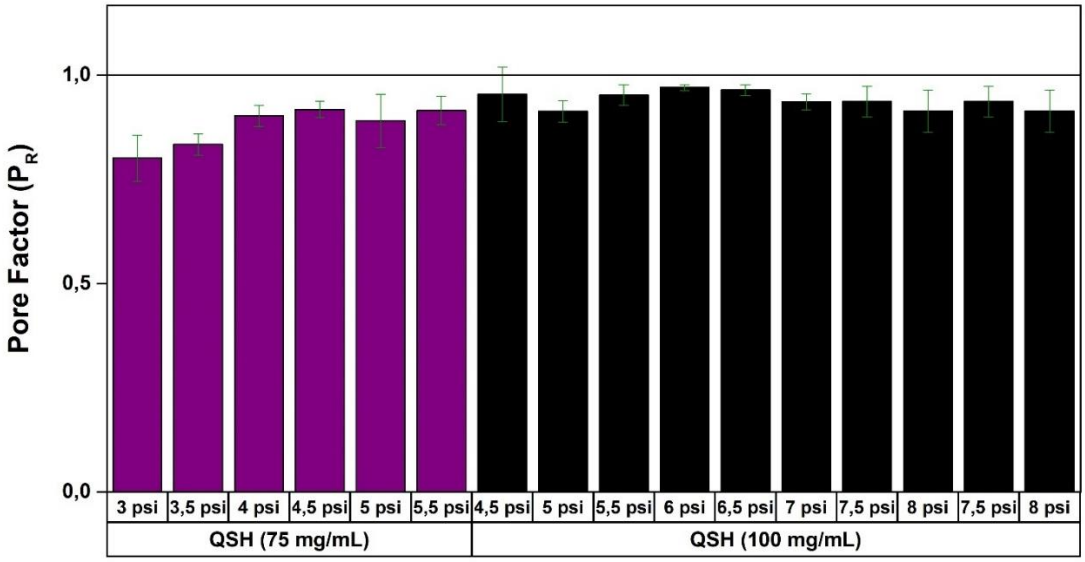

Figure 21. Pore factors of 75 and 100 mg/mL pristine QSH bio-inks between 3.0- 5.5 and 4.5- 8 psi pressure values, respectively.

For the production of porous structures with complex models, regular pores, uniform lines, and sharp junctions should be printed as exactly it was designed. Porous structures are needed for high cell viability. Therefore, regular pores with right angles of junctions should be obtained. The pore factor value was closer to 1 at 4.5 psi for 75 mg/mL pristine QSH and at 6.0 psi for 100 mg/mL pristine QSH. When the integrity and shape regularity of bioprinted constructs were examined and the closeness of pore factor values to 1 was taken into consideration (Figure 21), it can be said that 100 mg/mL pristine QSH had more convenient and repeatable results for bioprinting studies.

As expected, the viscosity increased with increasing bio-ink concentration. High-viscosity bio-inks are more controllable during bioprinting, due to the stability of bioprinted scaffolds (Yildirim and Arslan-Yildiz 2022).

After optimization of the bioprinting parameters, 100 mg/mL QSH was used for further QSH/Gel and P11-4/QSH/Gel bio-ink optimizations. Firstly, the filament model was bioprinted using these hybrid bioinks. Photos and microscope images of bioprinted filament models of QSH/Gel and P11-4/QSH/Gel are shown in Figure 22, and Figure 23, respectively.

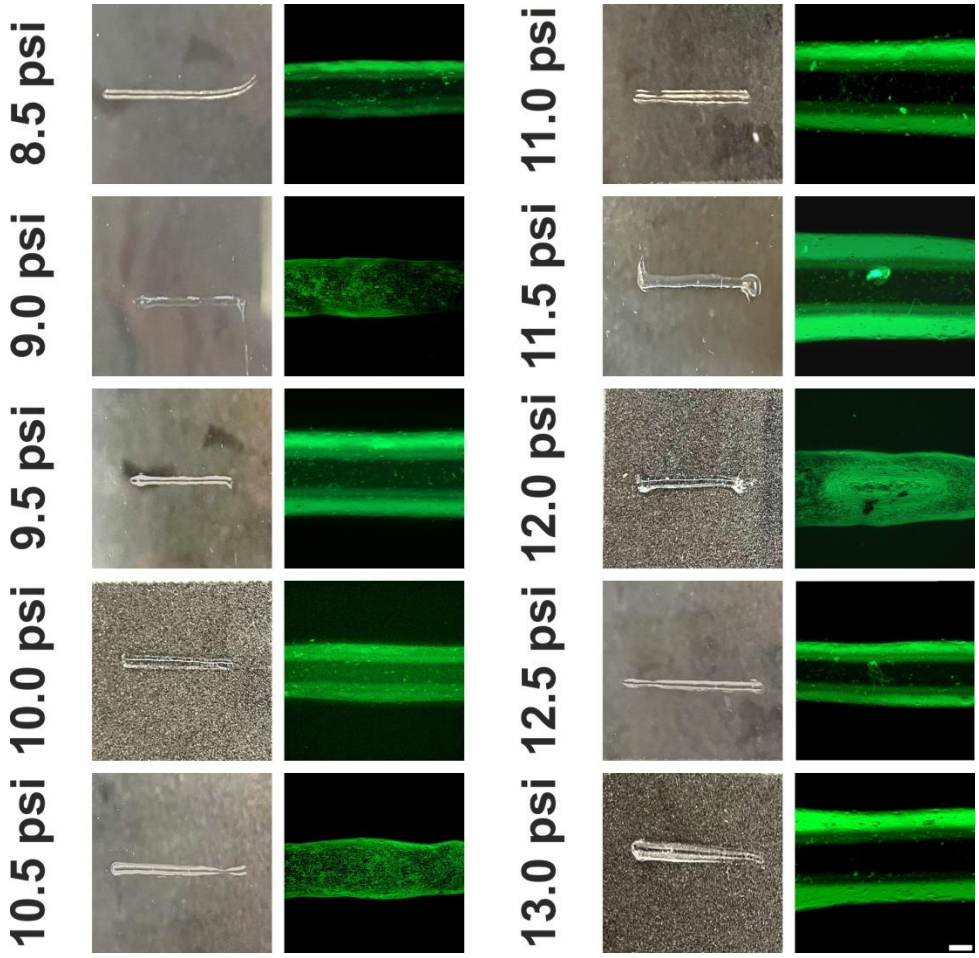

Figure 22. Bioprinting of QSH/Gel bio-ink as filament models using 25G tip between 8.5-13.0 psi pressure values. (Scale bar: 200 μm)

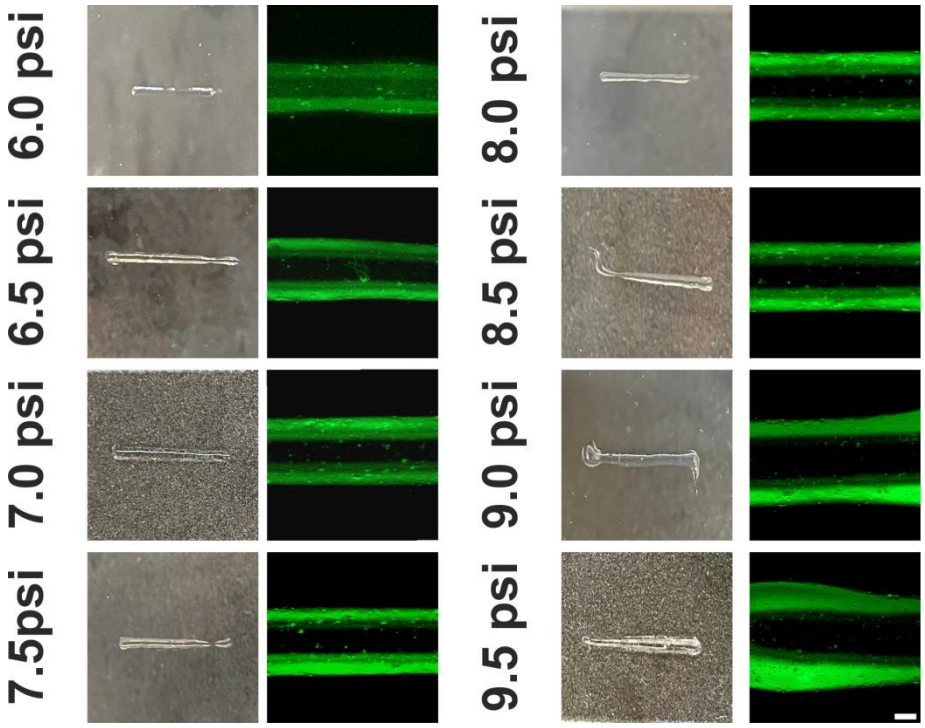

Figure 23. Bioprinting of P11-4/QSH/Gel bio-ink as filament models using 25G tip between 6.0-9.5 psi pressure values (Scale bar: 200 μm)

Bioprinting of QSH/Gel bio-ink has resulted in regular filaments between 9.5-11.5 psi, however, above 11.5 psi, the filaments became thicker and irregular. P11-4/QSH/Gel bio-ink produced regular filaments between 6.5-8.5 psi, but above 8.5 psi, the filament became thicker and irregular. Further, uniformity values of QSH, QSH/Gel, and P11-4/QSH/Gel bio-inks were calculated from these obtained images through Equation 1, and results are given in Figure 24. According to Figure 24, the uniformity value of QSH/Gel was closer to 1 at 9.5 psi and for P11-4/QSH/Gel, it was closer to 1 at 7.0 psi.

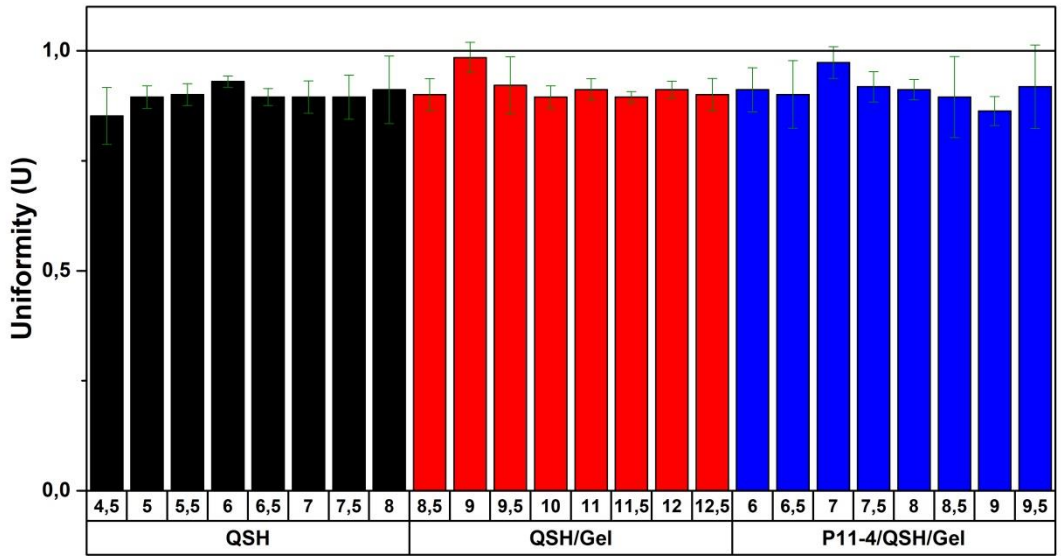

Figure 24. Uniformity analysis of 100 mg/mL pristine QSH bio-ink between 4.5 and 8.0 QSH/Gel bio-ink between 8.5 and 12.5, P11-4/QSH/Gel bio-ink between 6.0 and 9.5 psi.

Optimization of bioprinting parameters for QSH/Gel and P11-4/QSH/Gel was further conducted with bioprinting of square grid model by 25G dispensing tip for pressure values between 8.5-12.5 psi and 6.0-9.5 psi, respectively. Photos and fluorescence microscopy images of QSH/Gel and P11-4/QSH/Gel bio-inks are shown in Figure 25, and Figure 26, respectively.

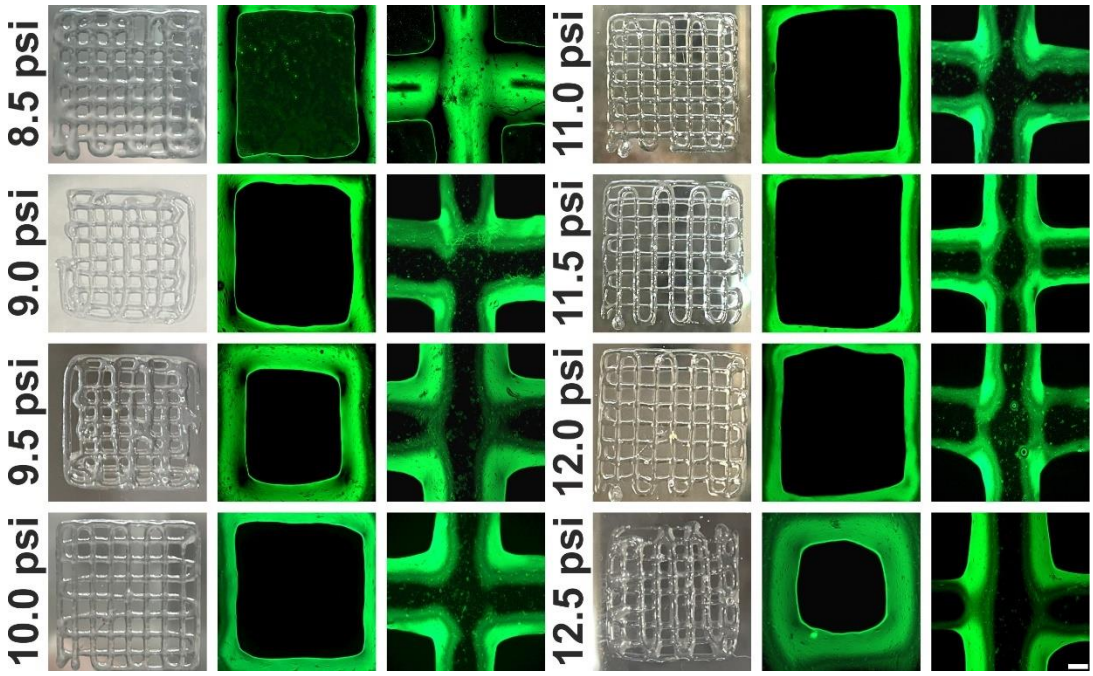

Figure 25. Bioprinting of QSH/Gel bio-ink as square grid model using 25G tip for 8.5 and 12.5 psi pressure range (scale bar: 200 μm).

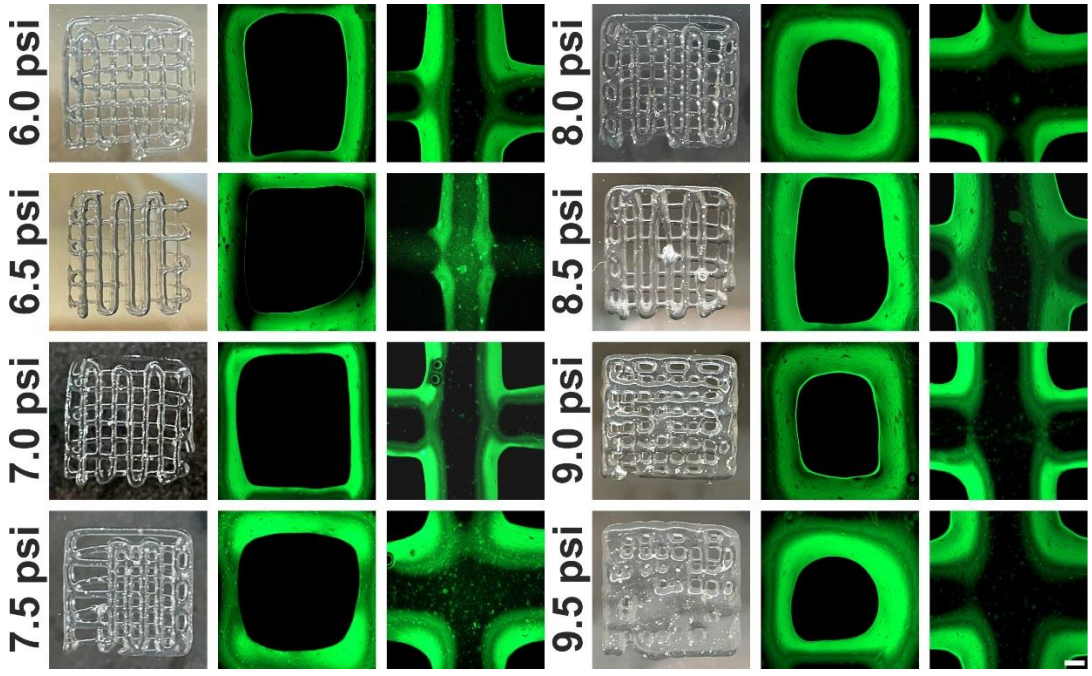

Figure 26. Bioprinting of P11-4/QSH/Gel bio-ink as square grid model using 25G tip for 6.0 and 9.5 psi pressure range (scale bar: 200 μm).

Pore factor values of pristine QSH, QSH/Gel, and P11-4/QSH/Gel bio-inks were calculated using Equation 2 and results are given in Figure 27.

The bioprinted square grid patterns of QSH/Gel and P11-4/QSH/Gel bio-ink had more regular pores when bioprinted with 8.5 psi and 7.0 psi, respectively. QSH/Gel bio-

ink was uniformly bioprinted between 8.5-12.0 psi (Figure 25), and P11-4-based QSH/Gel bio-ink was uniformly bioprinted between 7.0 and 8.0 psi (Figure 26). The pore factor value was closer to 1 at 9.0 psi and 7.0 psi for QSH/Gel and P11-4/ QSH/Gel bio-ink, respectively.

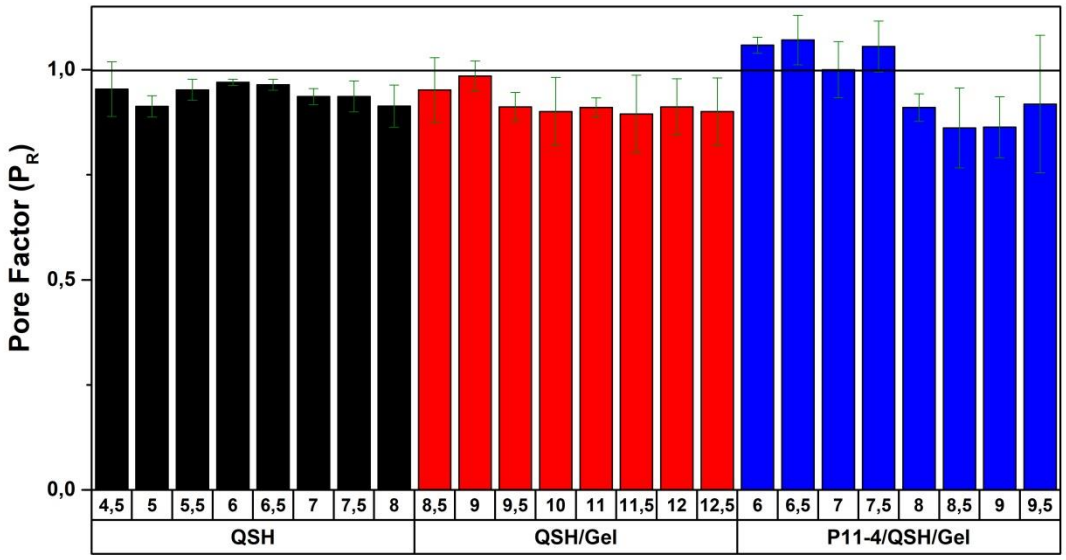

Figure 27. Pore factors of 100 mg/mL pristine QSH bio-ink between 4.5 and 8.0 psi, QSH/Gel bio-ink between 8.5- 12.5 psi and, P11-4/QSH/Gel bio-ink between 6.0- 9.5 psi pressure values.

In this study, the printing parameters of pristine QSH at different concentrations were optimized first, and it was seen that 100 mg/mL pristine QSH had suitable properties for 3D bioprinting (Figure 23 and Figure 27). As mentioned earlier, it is known that pristine Gelatin is thermally unstable, has poor mechanical properties and printability. It is not quite suitable for bioprinting and long-term cell culture studies due to the change in viscosity depending on temperature, and its poor mechanical properties. However, Gelatin is also known to be a promising biomaterial as a scaffold with its regenerative properties and high cell proliferation rate due to its chemical similarity to the ECM of native tissues. Also, its functional groups that allow modifications with other biomaterials or biomolecules, create advantages. For this reason, the bioprinting parameters of the QSH/Gelatin hybrid hydrogel were examined and it was observed that the Gel, which is not suitable for bioprinting in its pristine state, becomes a bioprintable material when mixed with QSH at a certain ratio. Thus, cell culture studies were carried out on these QSH/Gel bioprinted scaffolds by using optimized parameters. P11-4

synthetic peptide was also added as an additive to the QSH/Gel hydrogel to support mineralization in dental tissue. Therefore, printability analysis was carried out using P11-4/QSH/Gel bio-ink as abovementioned and bioprinting parameters were optimized. Bioprinting of P11-4/QSH/Gel bio-ink was performed around 7.0 psi.

3.3. Characterization of Bioprinted Scaffolds

Characterization of bioprinted pristine QSH, QSH/Gel and P11-4/QSH/Gel scaffolds was performed by swelling and protein adsorption analyses.

3.3.1. Swelling Analysis

Water uptake capacity determination was conducted by swelling test of bioprinted QSH, QSH/Gel and P11-4/QSH/Gel scaffolds (Figure 28).

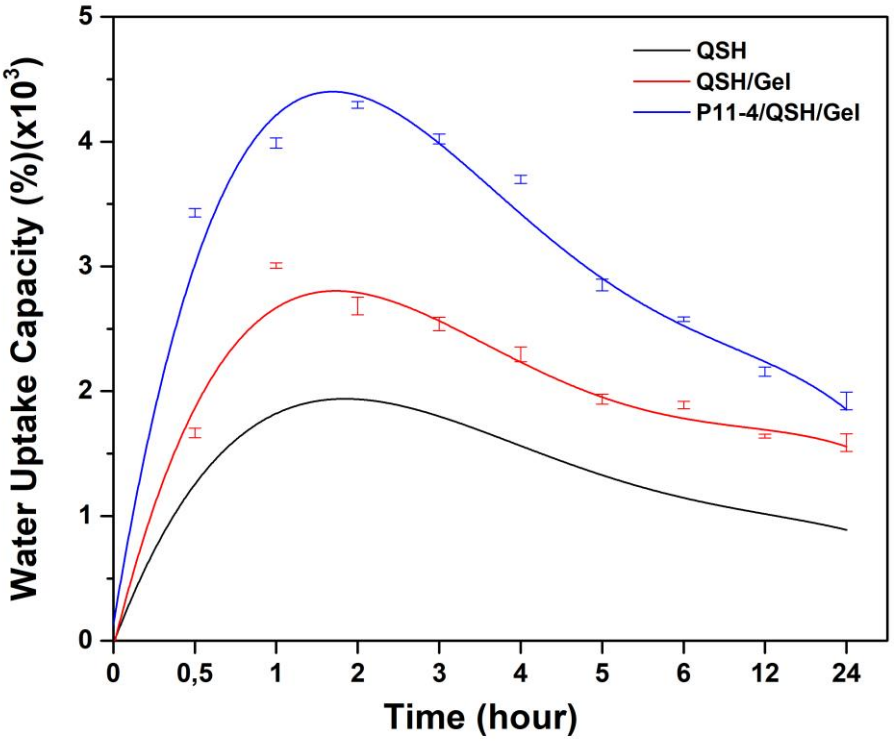

Figure 28. Water uptake capacity of pristine QSH, QSH/Gel, and P11-4/QSH/Gel scaffolds.

The swelling process depends on physicochemical parameters so mechanical properties change during this process. The hydrophilic parts of the biopolymer network become more elastic and expand. At the equilibrium of swelling, the elastic forces of the polymer backbone cancel the osmotic forces caused by water.

The maximum swelling was achieved around the first two hours for QSH scaffolds. Till the 1st hour, water holding capacity was increased proportionally, and it reached the maximum point around the 2nd hour, later deswelling occurred. Maximum water holding capacity was achieved at 2nd hour, especially for P11-4/QSH/Gel scaffold. Since the P11-4 peptide is a water-soluble peptide, the time-dependent dissolution of the P11-4 peptide might lead to physical changes in the structure.

Pristine QSH, QSH/Gel, P11-4/QSH/Gel scaffolds hold 15.6, 17, 21.6 times more H_2O than their own mass when kept in water for 6 hours, and 12, 15.6, 18.1 times after 24 hours of incubation in water, respectively. Pristine QSH contains hydrophilic functional groups since it is highly composed of glucuronoxylan. Additionally, glucuronic acid and xylose parts of glucuronoxylan have high water uptake properties due to their hydrophilic functional groups such as carboxylic acid and hydroxyl. Gelatin is a collagen derivative that holds high amounts of water through its amino groups. In literature it was reported that P11-4 peptide forms as antiparallel β-sheet structure under pH 7.5 and it has -COOH and -NH_2 groups in amino acid sequence that led it to hold high volumes of water (Kyle et al.), which is also correlated with our study. These results show that bioprinted hydrogel scaffolds have remarkable water uptake capacities.

3.3.2. Protein Adsorption

Investigation of protein adsorption on scaffolds is very important to acquire information about cell adhesion since cells adhere to the surfaces through proteins. A protein adsorption assay was used to determine the amount of adsorbed protein on pristine QSH, QSH/Gel, and P11-4/QSH/Gel scaffolds. The standard curve was plotted using the absorbance values of known BSA concentrations (Figure 29.). Then, the amount of adsorbed proteins were quantified *via* a calibration curve and the results are given in Figure 30.

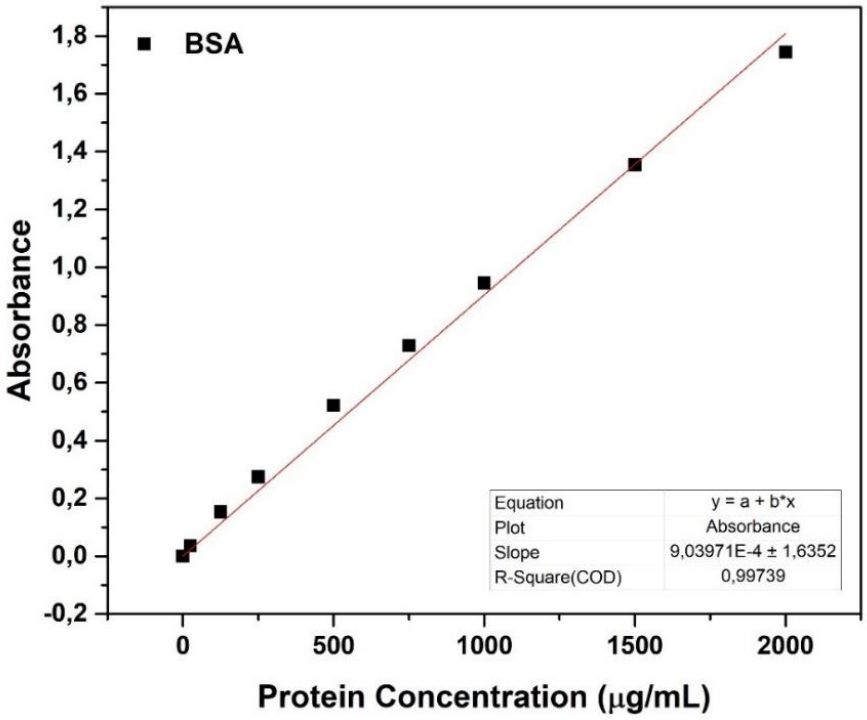

Figure 29. Standard curve of BSA.

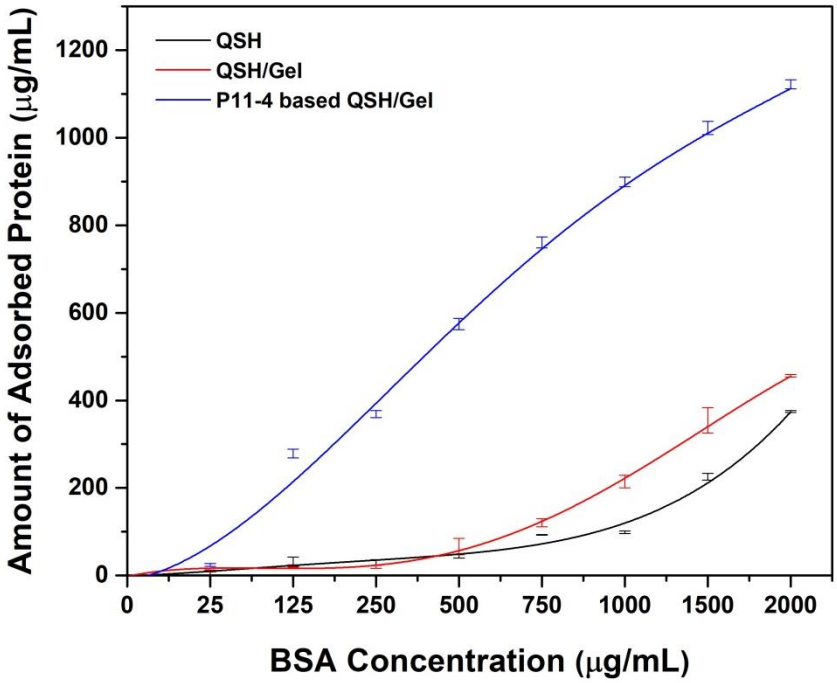

Figure 30. Protein adsorption graph of pristine QSH, QSH/Gel, and P11-4/QSH/Gel.

According to Figure 30, considerably high BSA adsorption was observed for pristine QSH, QSH/Gel, and P11-4/QSH/Gel scaffolds at 2000 μg/mL BSA concentration. The addition of Gelatin into QSH resulted in increased protein

adsorption, and P11-4 peptide addition led to the adsorption of approximately 1100 μg/mL protein. These findings indicate that the presence of both Gelatin and P11-4 peptide increased the protein adsorption and would increase cell attachment during cell culture studies. In the literature, Koch et al. demonstrated that each self-assembling peptide composition would affect the hydrogel characteristics by changing the surface charge for higher adsorption of proteins (Koch et al. 2020). Also, increasing the peptide concentration resulted in a higher density network in hydrogel structures that could absorb high amount of protein (Koutsopoulos 2016). As a result of this analysis, increasing protein adsorption was observed especially for peptide-containing hydrogels that correlated with the literature.

3.4. Cell Culture Studies

SaOS-2 human osteosarcoma cell line was used for 2D and 3D cell culture studies. Cell viability and proliferation analyses of SaOS-2 cells were carried out with Live/Dead and MTT assays.

3.4.1. 2D Cell Culture and Maintenance

Cancer cell lines have a higher proliferation profile than healthy cell lines and are considered more durable in cell culture. SaOS-2 cell line (human osteosarcoma cell line) is commonly used in hard tissue engineering applications as a model. Some of the advantages of using the SaOS-2 cell line are that they can replicate, are immortal, and easily obtain large numbers of cells in a short time and are highly resistant to changes in cell culture studies. Also, the ability of SaOS-2 cells to express and deposit a mineralized ECM makes these cells a valuable model for studying dental and bone tissue models. Here, the cell proliferation rate and efficiency of SaOS-2 cells were determined by MTT assay, and the viability of 2D monolayer cells was evaluated by Live/Dead assay. 2D cell culture systems are used as reference models for 3D cell culture studies. Thus, the behaviour of the cell line and the resistance to long-term culture can be seen.

On day 1, 3, 5, 7, 9, 11, 13, 15, 21, and 28 Live/Dead and MTT assays were performed to evaluate the viability of cells as given in Figure 31 and Figure 32, respectively.

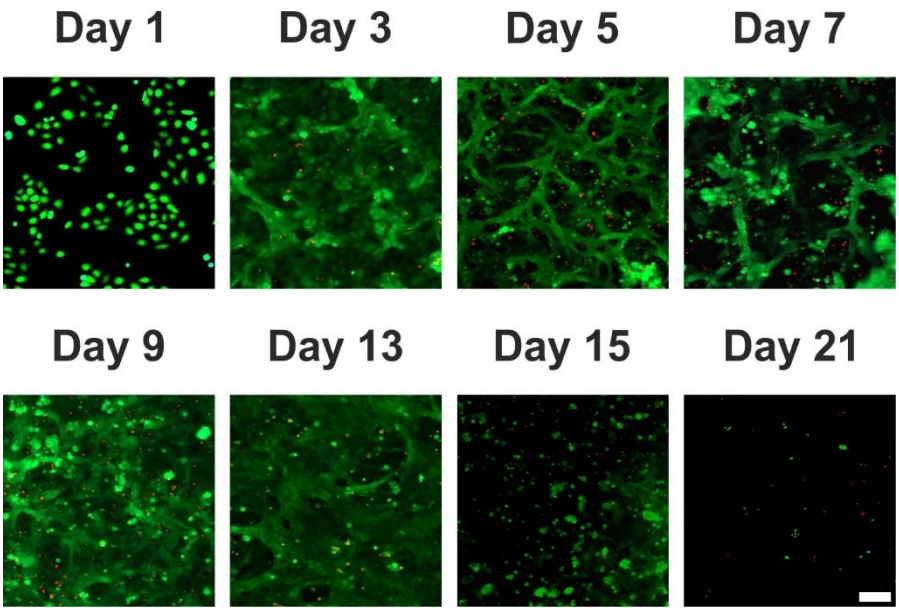

Figure 31. Live/Dead assay results of cells on 2D monolayer (green: live cells, red: dead cells).

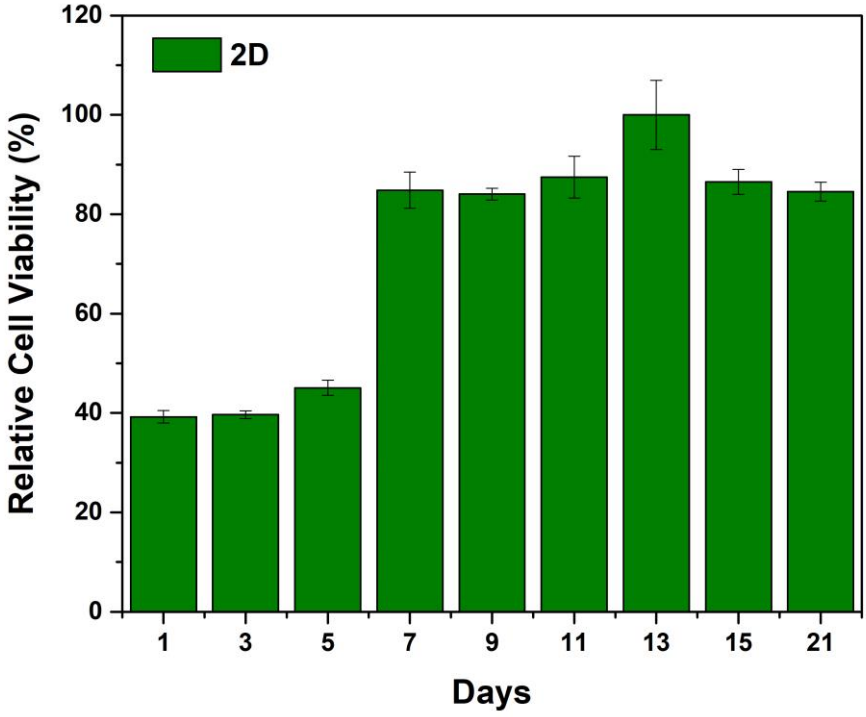

Figure 32. Cell viability results of 2D SaOS-2 cells evaluated by MTT assay for long-term culture.

According to the relative cell viability values of long-term cultured SaOS-2 cells (Figure 31 and Figure 32), the cell viability rate was increased till day 13 and then started to decrease. After day 13, monolayered cells started to make multilayers and detach from the surface. This can be the reason for the decrease in viability results. In 2D cell culture studies, it is commonly seen that the cells start to lose their viability by detaching from the surface after day 7 the contrary of the SaOS-2 cell line. Although the SaOS-2 cell line is more durable and proliferating than healthy cells and many other cancer cell lines, they could not be cultured on a 2D monolayer for long term, which is also supporting the idea that 3D cell culture studies are necessary for long-term studies and applications.

3.4.2. 3D Cell Culture Studies

3D cell culture studies of SaOS-2 cells on bioprinted hydrogel scaffolds were conducted by cell viability and proliferation analysis via Live/Dead and MTT assays. In addition, characterization of 3D cell culture was carried out by mineralization and cellular/extracellular component analyses with Alizarin Red Staining and Immunostaining assays, respectively.

3.4.3. Cell Viability Analysis on 3D Cell Culture

Cell viability of short- and long-term cultured SaOS-2 on 3D bioprinted pristine QSH scaffolds were investigated by performing Live/Lead and MTT analyses.

Cell viability and cell number optimization studies were started using bioprinted 75 mg/mL pristine QSH scaffolds. $2x10^5$, $5x10^5$, and $1x10^6$ SaOS-2 cells were seeded on bioprinted constructs. Live/Dead analysis was performed to observe cell viability on 75 mg/mL bioprinted pristine QSH on days 1, 3, 5, and 7, and results are given in Figure 33.

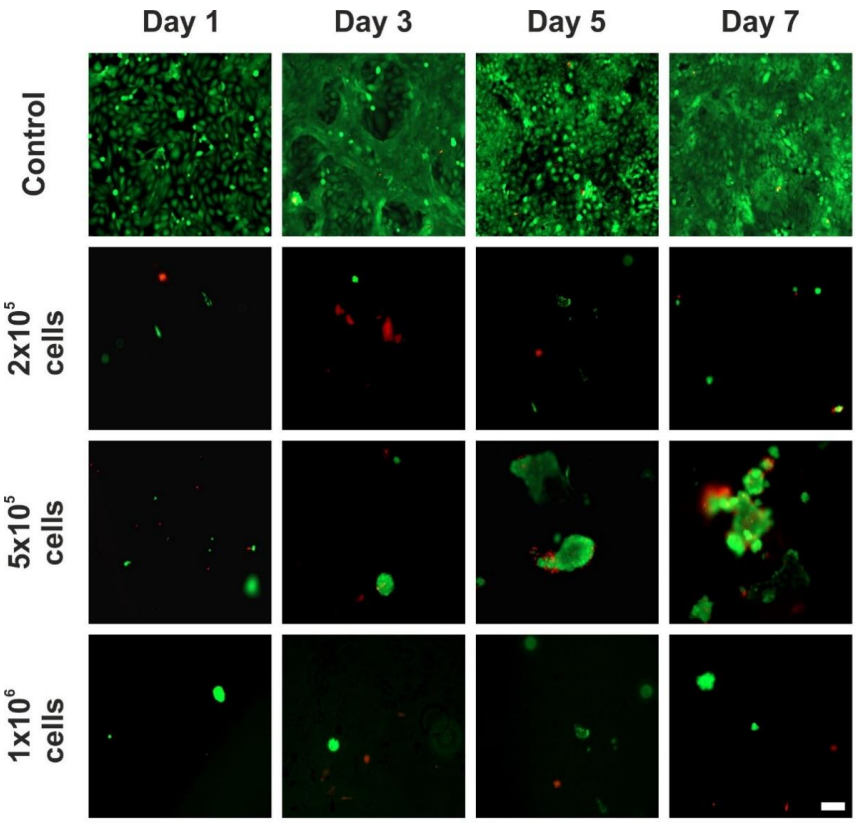

Figure 33. Representative Live/Dead assay results of $2x10^5$, $5x10^5$ and $1x10^6$ SaOS-2 cells seeded on bioprinted 75 mg/mL pristine QSH (scale bar: 100 μm) (green: live cells, red: dead cells).

According to Figure 33, the highest cell proliferation was observed in the 3D group which has $5x10^5$ cell number compared to other experimental groups for 7 days of incubation. Then, Live/Dead analysis was performed to observe cell viability on 100 mg/mL bioprinted pristine QSH scaffolds on days 1, 3, 5, and 7, and results are given in Figure 34.

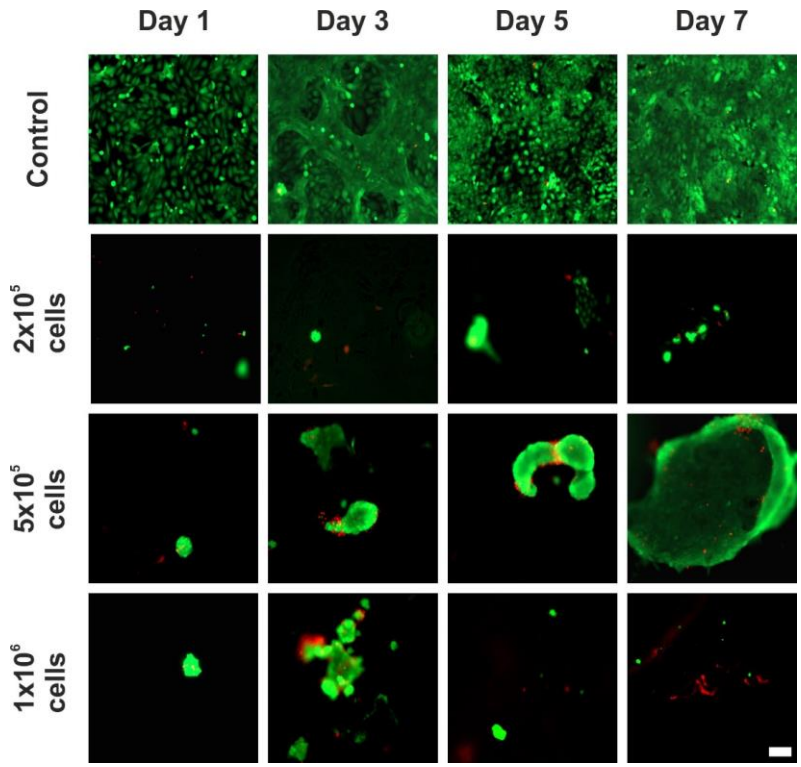

Figure 34. Representative Live/Dead assay results of $2x10^5$, $5x10^5$ and $1x10^6$ SaOS-2 cells on bioprinted 100 mg/mL pristine QSH (scale bar: 100 μm) (green: live cells, red: dead cells).

According to the results that are given in Figure 34, the highest cell viability was obtained at day 7 with $5x10^5$ cell number. Bioprinted constructs with $2x10^5$ and $1x10^6$ cell numbers did not show a significant increase in cell proliferation during the 7-day culture. As a result of these experiments, it was decided that using only QSH as a scaffold material does not provide an adequate environment for the adhesion of SaOS-2 cell proliferation. This could be caused by the variation in quince seed content from batch to batch, as seen in other natural hydrogels. To increase the cell attachment, Gelatin hydrogel was added in QSH.

5:1 QSH/Gel scaffolds were obtained by bioprinting and, 3D cell culture studies were performed on 5:1 QSH/Gel constructs. $2x10^5$, $5x10^5$, and $1x10^6$ SaOS-2 cells were seeded on QSH/Gel (5:1) scaffolds, then, Live/Dead analysis was performed to observe cell viability on days 1, 3, 5, and 7 as given in Figure 35.

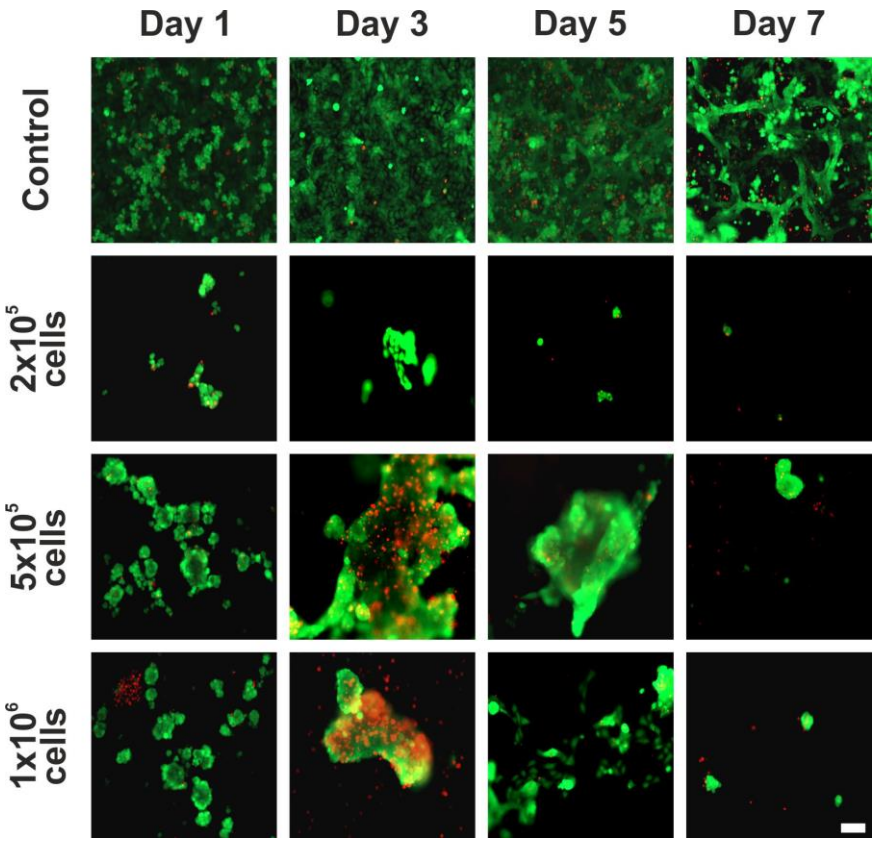

Figure 35. Representative Live/Dead assay results of $2x10^5$, $5x10^5$ and $1x10^6$ SaOS-2 cells on bioprinted QSH/Gel (5:1). (Scale bar: 100 μm) (green: live cells, red: dead cells).

Phase and viscosity of Gel change depending on temperature. Therefore, bioprinting parameters were constantly changed due to the viscosity of Gelatin and this was an unexpected situation for optimization of the printing parameters. During bioprinting of QSH/Gel (5:1), the Gelatin caused unstable, non-homogeneous, and non-uniform scaffolds. Hence, the bioprinted scaffolds disintegrated and could not be removed easily from the printbed. Despite this, cells were seeded on these scaffolds, if they were disintegrated, and then $2x10^5$, $5x10^5$, and $1x10^6$ SaOS-2 cells were seeded on these scaffolds to observe the effect of Gel addition to QSH. According to Figure 35, it can be said that Gel addition to QSH resulted in a positive effect on cell viability and proliferation. After day 5, constructs disintegrated completely, and the surface area of hydrogel decreased compared to other days. Therefore, Live/Dead images could not be taken homogenously. By looking at the increase in the cell number, the studies were continued by keeping the $5x10^5$ SaOS-2 cell number constant. Additionally, Gel addition increased cell viability, but the Gelatin proportion of hybrid hydrogel resulted

in obstruction of bioprinting. Therefore, the Gel ratio was decreased and 10:1 QSH/Gelatin scaffolds were bioprinted for further 3D cell culture studies.

Furthermore, pristine QSH and Gel were mixed with a 10:1 ratio and then bioprinted. SaOS-2 cells were seeded on these bioprinted scaffolds with $5x10^5$ cell number/well. Cell viability and proliferation of cells were evaluated on days 1, 3, 5, 7,9, 11, 15, and 21, and results are given in Figure 36. Here pristine QSH was used as a 3D control group.

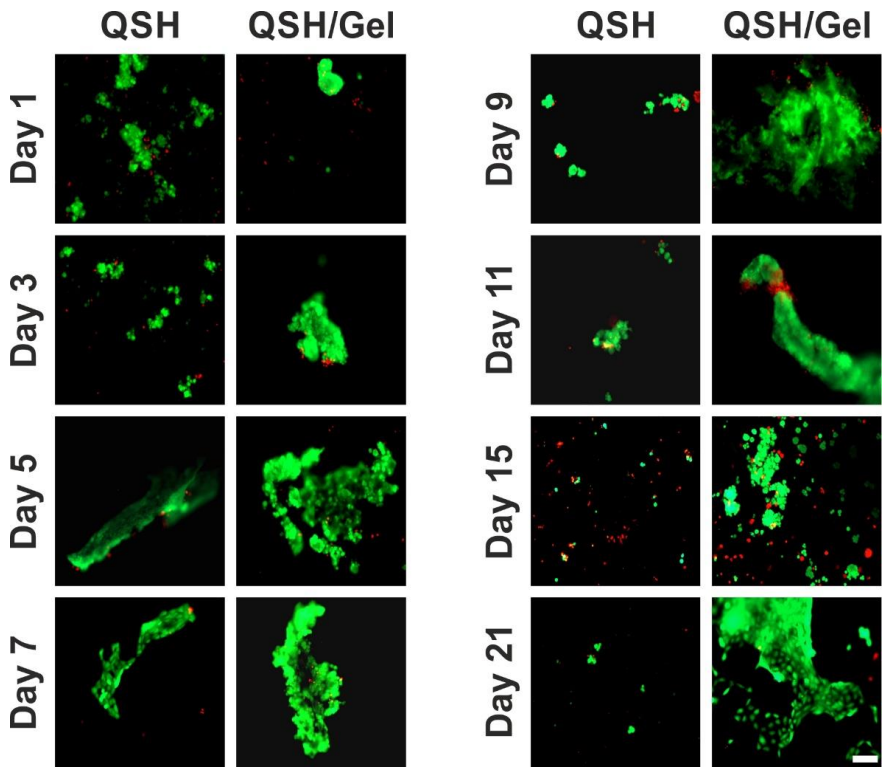

Figure 36. Representative Live/Dead assay results of $5x10^5$ SaOS-2 cells on bioprinted QSH/Gel (10:1) and 100 mg/mL pristine QSH scaffolds were used as 3D control (scale bar: 100 μm) (green: live cells, red: dead cells).

Live/Dead assay results of SaOS-2 cells seeded on bioprinted QSH/Gel (10:1) and pristine QSH were given in Figure 36. Bioprinted QSH scaffolds were used as 3D control in this experiment to compare the effect of Gel addition on cell adhesion and viability. According to Live/Dead assay results, cell viability increased dramatically on QSH/Gel scaffolds till day 21 when we compared pristine QSH and QSH/Gel samples. According to the long-term cell culture studies, QSH/Gel (10:1) scaffolds showed the highest cell viability and proliferation rate so far, and these scaffolds remained stable

for 21 days without disintegration in the culture medium. Therefore, the P11-4 peptide addition was done by utilizing the same experimental parameters.

P11-4 peptide was used to increase mineralization on bioprinted QSH/Gel scaffolds. 100 and 200 μM P11-4/QSH/Gel scaffolds were bioprinted and $5x10^5$ SaOS-2 cells were seeded on these scaffolds. Cell viability was evaluated by Live/Dead assay on days 1, 3, 5, and 7. Cell viability on P11-4/QSH/Gel scaffolds was compared with QSH/Gel as 3D control and results are given in Figure 37.

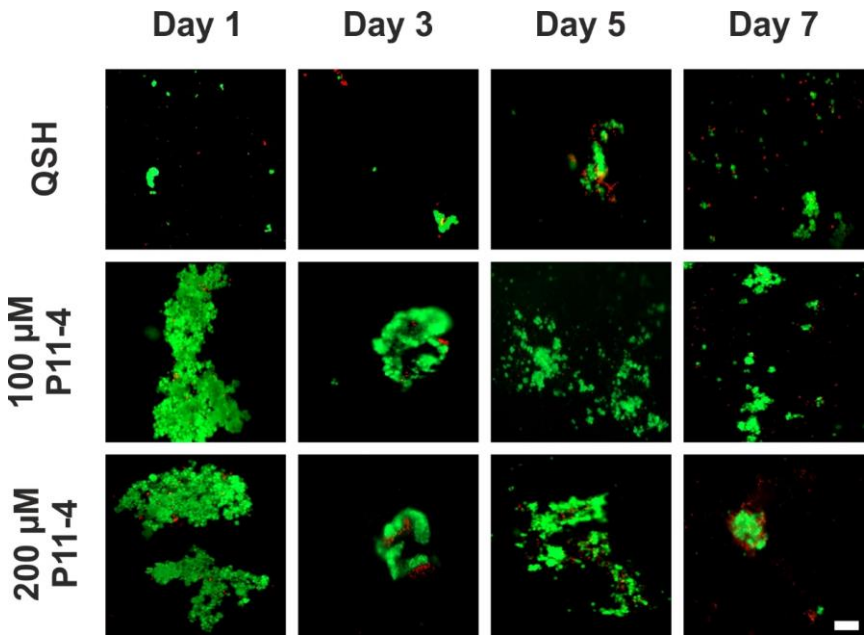

Figure 37. Representative Live/Dead assay results of $5x10^5$ SaOS-2 cells on bioprinted 100 and 200 μM P11-4/QSH/Gel. Bioprinted QSH/Gel scaffolds were used as 3D control (scale bar: 100 μm) (green: live cells, red: dead cells).

Cell viability on both 100 and 200 μM P11-4/ QSH/Gel was high compared to 3D control (QSH/Gel) on day 1. Then, cell viability on P11-4/QSH/Gel group was decreased day by day. Homogenization was an obstacle during the preparation of hybrid hydrogels, due to the small volumes of hydrogels. This problem caused non-homogeneous hybrid scaffold formation; thus, non-homogeneous cell growth was observed when these scaffolds were utilized. Also, it was predicted that conditioning the scaffolds for 24h might cause the non-crosslinked peptide to dissolve in the culture medium. In order to understand the effect of the conditioning procedure during cell culture, 100 μM P11-4/QSH/Gel scaffolds were prepared for cell culture experiments, both by conditioning and non-conditioning.

3D cell culture studies were carried out on bioprinted pristine QSH, QSH/Gel, conditioned and unconditioned P11-4/QSH/Gel scaffolds and cell viability was evaluated on days 1, 3, 5, 7, 9, 11, 13, 15, 21, and 28. Live/Dead assay results are given in Figure 38.

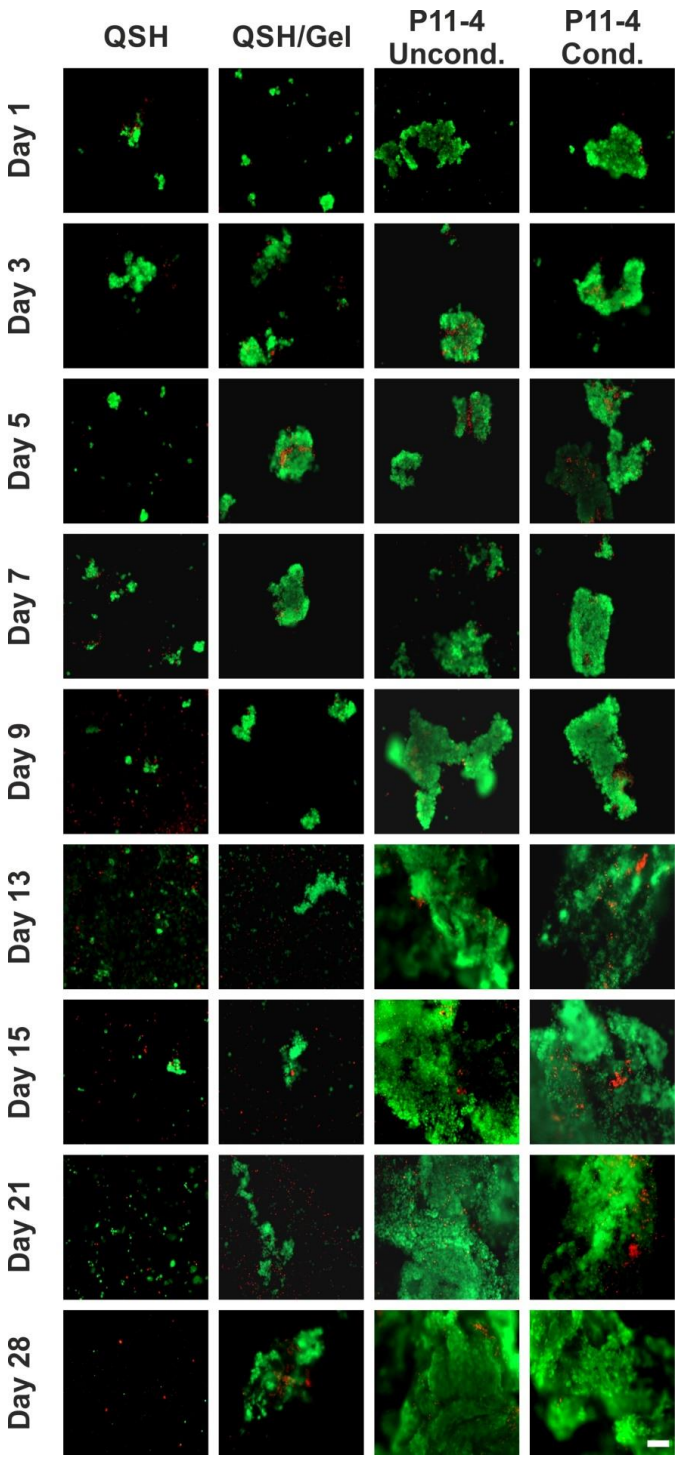

Figure 38. Representative long-term Live/Dead assay results of $5x10^5$ SaOS-2 cells seeded on pristine QSH, QSH/Gel, conditioned (cond.) and unconditioned (uncond.)

100 μM P11-4/QSH/Gel scaffolds. Bioprinted pristine QSH and QSH/Gel scaffolds were used as 3D control (scale bar: 100 μm) (green: live cells, red: dead cells).

3.4.3.1. MTT Assay

Viability of SaOS-2 cells was also evaluated by MTT assay. MTT assay was performed on day 1, 3, 5, 7, 9, 11, 13, 15, 21 and 28. The results are given in Figure 39.

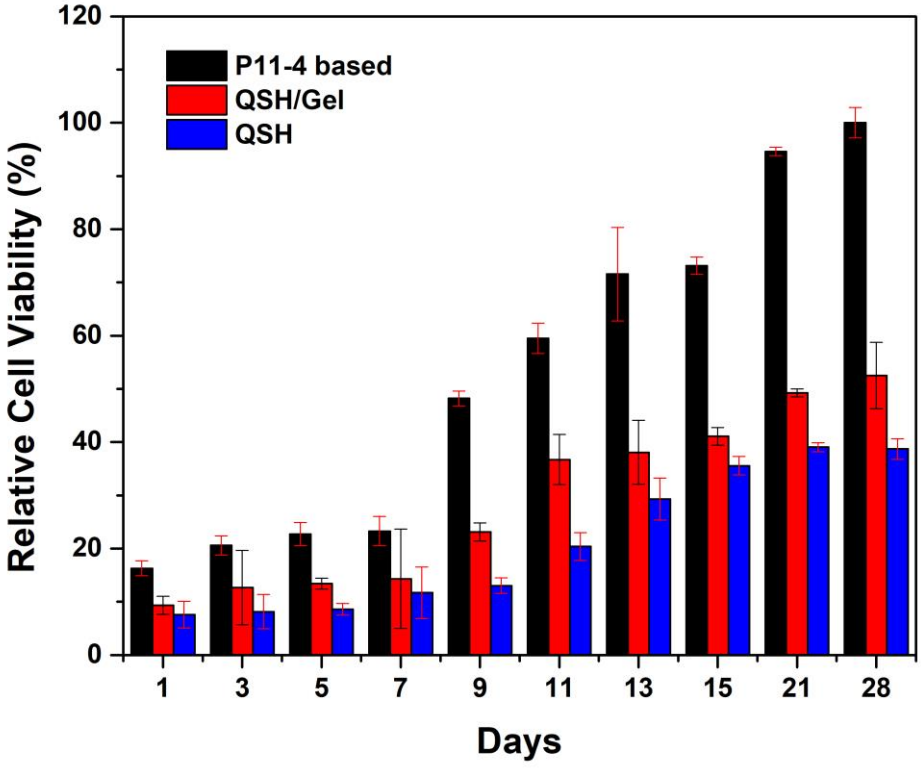

Figure 39. MTT assay results of SaOS-2 cells on pristine QSH, QSH/Gel, P11-4/QSH/Gel for long-term.

According to the MTT assay results, which are given in Figure 39, it can be said that cell viability increased day by day for all scaffolds. Cell viability on pristine QSH was increased till day 15. However, no significant increase was observed between days 15, 21, and 28. This means cells reached maximum viability. In addition to these results, higher cell viability was observed on QSH/Gel scaffolds on day 28. Nevertheless, the difference in relative cell viability results was not remarkable. After day 7, cell viability increased dramatically on P11-4/QSH/Gel scaffolds. The reason might be the beginning

of mineralization and the osteosarcoma cells' affinity for a mineralized environment to proliferate much more. Additionally, on day 21 and 28 the cell viability on P11-4/QSH/Gel were extremely high, and the results of the mineralization assay also prove that the cells show a greater increase on mineralized scaffolds.

As a result, SaOS-2 cells had higher cell viability rates on QSH/Gel scaffolds compared to pristine QSH scaffolds; because Gel addition increased the protein content of the scaffold, and cells prefer ECM-like scaffolds to adhere. Since the ECM of native tissues contains a high amount of Collagen, QSH/Gel creates a more similar microenvironment for cells. With the addition of polysaccharides to Gelatin, the mixture is becoming more advantageous in mimicking the ECM, which largely contains proteoglycans or glycoproteins. Also, Afewerki et. al mentioned that 3D Gelatin/polysaccharide scaffolds have benefits such as similarity to ECM (Afewerki et al. 2019). In addition to these advantages of Gelatin/polysaccharide hydrogels, peptide-based hydrogels have been proven to be fascinating biomaterials due to their great biocompatibility and high protein content. The ability of peptide-based hydrogels to provide extracellular matrix-mimicking environments for their use in tissue engineering applications. In parallel to this information, the highest cell viability was obtained with P11-4/QSH/Gel scaffold compared to pristine QSH and QSH/Gel. These results prove that the P11-4/ QSH/Gel scaffold is suitable especially for dental tissue engineering applications.

3.4.4. Alizarin Red Staining for Mineralization Analysis

Mineralization assay was performed on QSH, QSH/Gel, and P11-4/QSH/Gel scaffolds. SaOS-2 cells were cultured for 28 days, and mineralization was analyzed on day 1, 3, 5, 7, 9, 11, 13, 15, 21, and 28. Alizarin Red Staining was performed. Mineralization was observed by fluorescence microscopy and results are given in Figure 40.

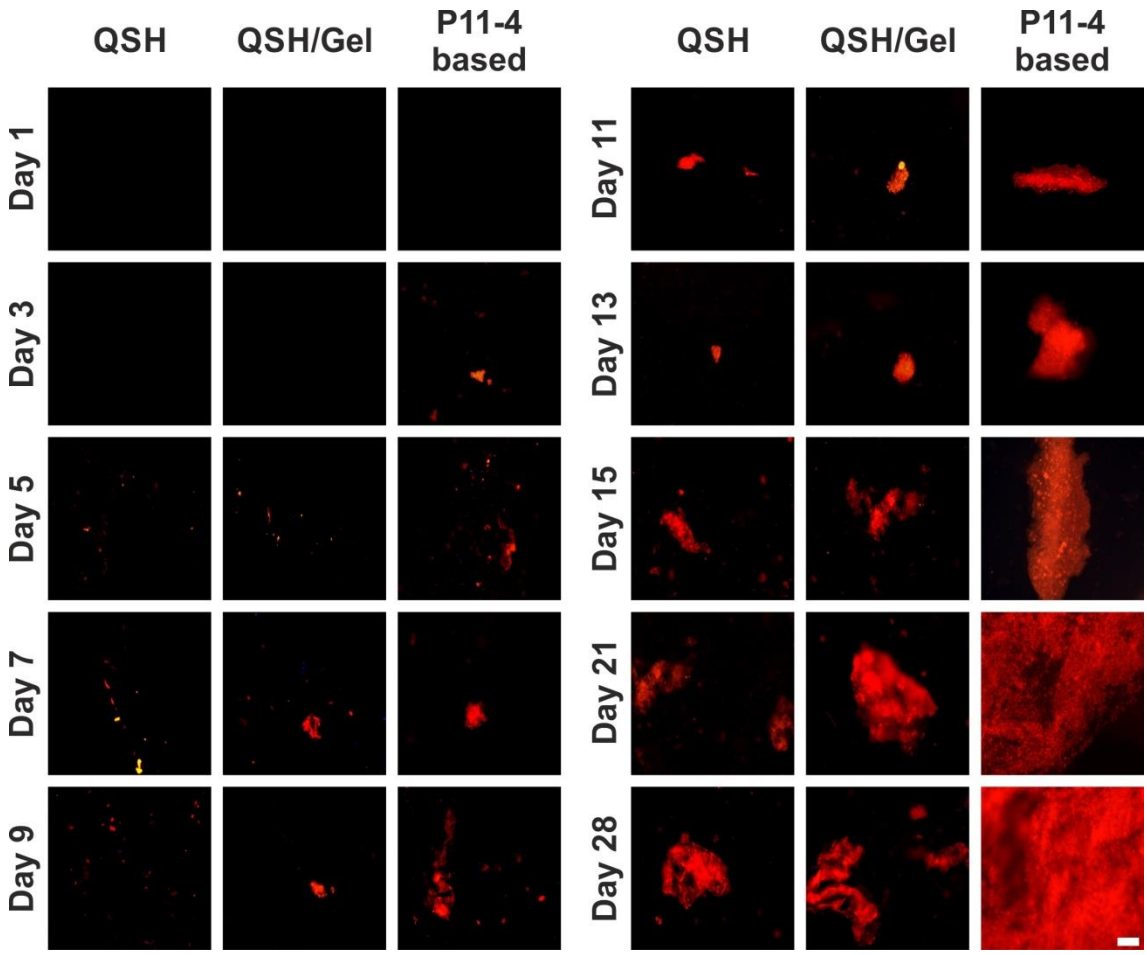

Figure 40. Mineralization assay for 28 days SaOS-2 cultured pristine QSH, QSH/Gel and P11-4/QSH/Gel scaffolds. Alizarin Red Staining was used to indicate the calcified areas on all bioprinted scaffolds.

As is seen in Figure 43, on day 3 mineral formation was started for SaOS-2 cells seeded on P11-4/QSH/Gel and on day 5 for other constructs. As SaOS-2 is a human osteosarcoma cell line, it has alkaline phosphatase activity and the ability to secrete the hormone osteocalcin, which is responsible for the synthesis and mineralization of hard-structured tissues such as bone and tooth matrix. Mineral formation takes time due to the life cycle of cells and their adaptation period to the environment. When the cell attachment and adaptation took place, cells began to form calcium phosphate minerals. The P11-4 peptide is designed to promote the formation of *de novo* hydroxyapatite crystals on its surface by increasing net mineral gain. Sousa et al. reported that the P11-4 peptide interacts with collagen type I, by preventing collagen proteolysis increasing the resistance of collagen fibers and improving stability. According to Dawasaz et al. with the addition of P11-4 peptide to hybrid hydrogel mineralization was assessed (Dawasaz et al. 2022b). Similarly, in this study

mineralization was observed by the ARS method on all scaffolds. The addition of the P11-4 peptide increased the mineralization since P11-4 is a self-assembling and biocompatible peptide that is designed to use in dental tissue engineering studies due to its proper amino acid sequences to the native dental tissue. P11-4 peptide can form a 3D hydrogel and the have ability to form hydroxyapatite crystals which is obligatory to form dental tissue. Therefore, although mineral formation was also seen in QSH, QSH/Gel as in P11-4/QSH/Gel scaffolds, the highest mineralization was observed for P11-4/QSH/Gel scaffolds.

3.4.5. SEM and EDX Analyses

SEM and EDX analyses of long-term cell cultured QSH/Gel, P11-4/QSH/Gel scaffolds were performed to observe mineral formation. SaOS-2 cells are odontoblast-like cells, and they have the ability to bind Ca^{+2} (Bozycki et al. 2018). Here, *de novo* formation of HAP crystals occurred, and mineralization was observed on both cell-cultured QSH/Gel and P11-4/QSH/Gel scaffolds (Figure 41). These results prove that increased mineral formation can be obtained with the addition of P11-4 peptide, which correlates with the literature. The higher mineral deposition was observed on P11-4/QSH/Gel scaffolds due to *in situ* nucleation of HAP to the QSH/Gel scaffolds. Also, P11-4 peptide has an effect on increasing the mineral density and formed minerals was accumulated and spread on to the scaffold day by day.

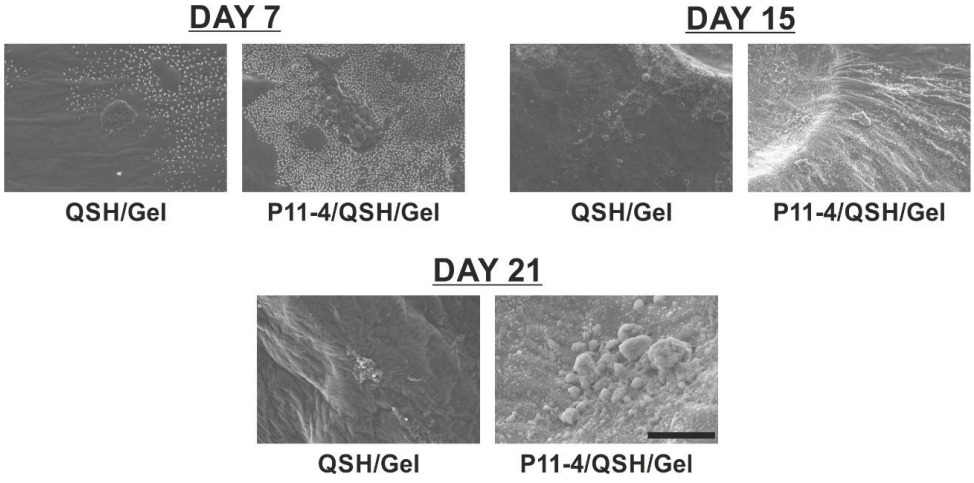

Figure 41. SEM images of long-term cell cultured QSH/Gel and P11-4/QSH/Gel scaffolds. (Scale bar: 30 μm)

EDX analysis was performed to analyze the chemical compositions of cell-cultured QSH/Gel and P11-4/QSH/Gel scaffolds. As a result of this experiment, it was

seen that scaffolds contain elements such as C, O, Ca, P, and Na. Due to the odontoblast-like cell behaviour of SaOS-2 cells, Ca^{+2} formation was observed on all samples (Figure 42 and Figure 43). Araújo et. al. stated that P11-4 peptide induced mineral deposition comparable to native protein involved in biomineralization (Araújo et al. 2022). Combined with its ability to bind type I collagen, P11-4 is a promising bioinspired molecule that provides native-tissue conditions for dental tissue formation. As mentioned above, with the addition of the P11-4 peptide, higher Ca^{2+} formation was observed in P11-4/QSH/Gel scaffolds compared to QSH/Gel scaffolds and increased up to day 28 as expected (Figure 44).

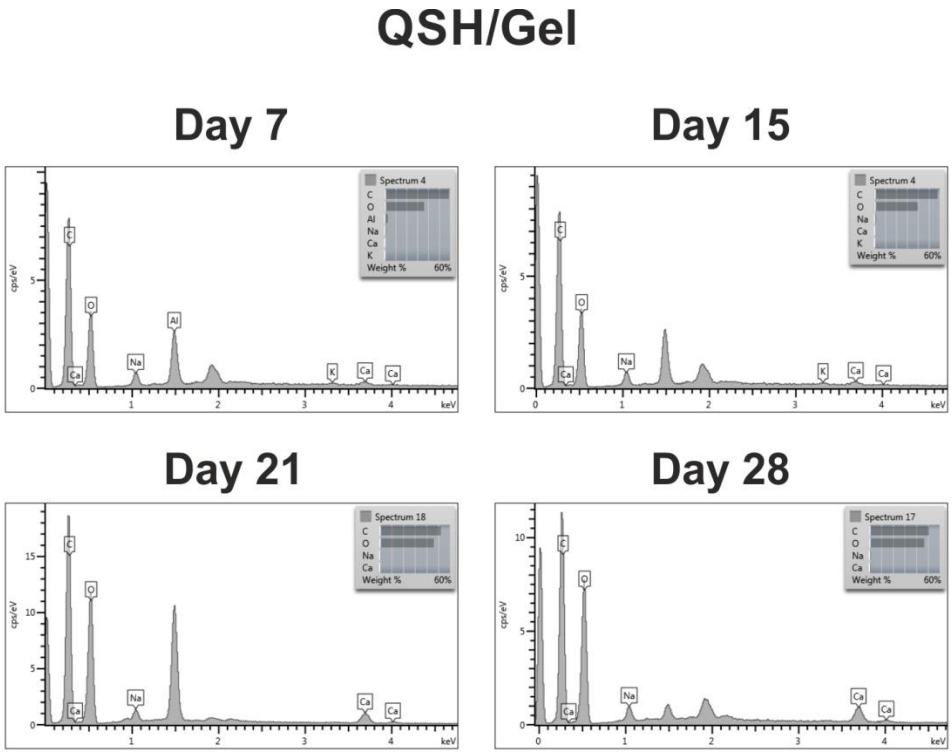

Figure 42. EDX results of long-term cell cultured QSH/Gel scaffolds.

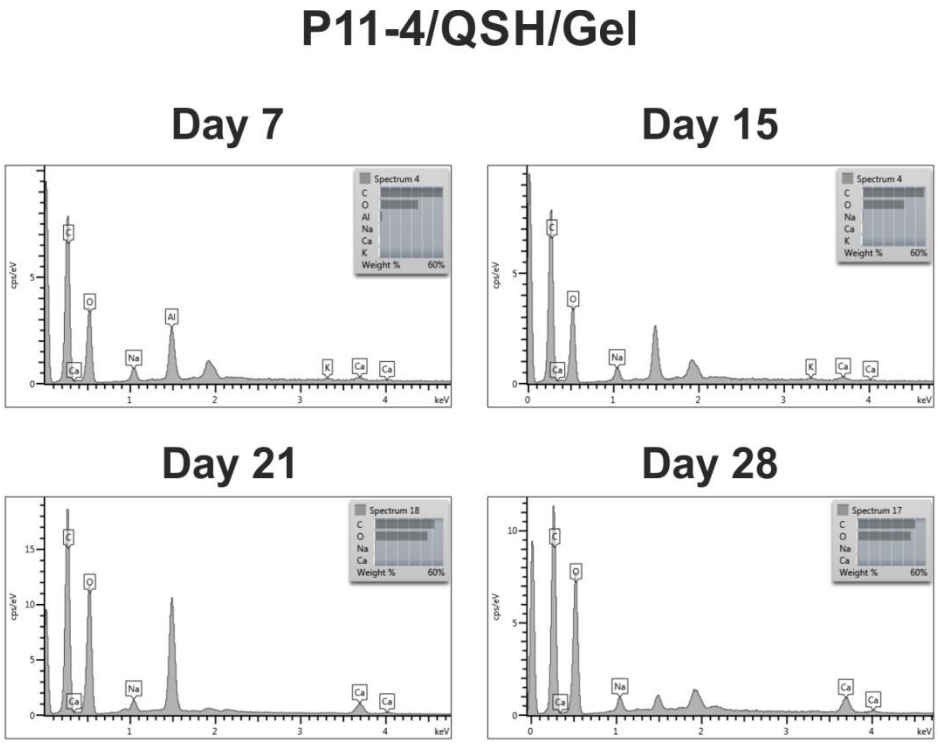

Figure 43. EDX results of long-term cell cultured QSH/Gel and P11-4/QSH/Gel scaffolds.

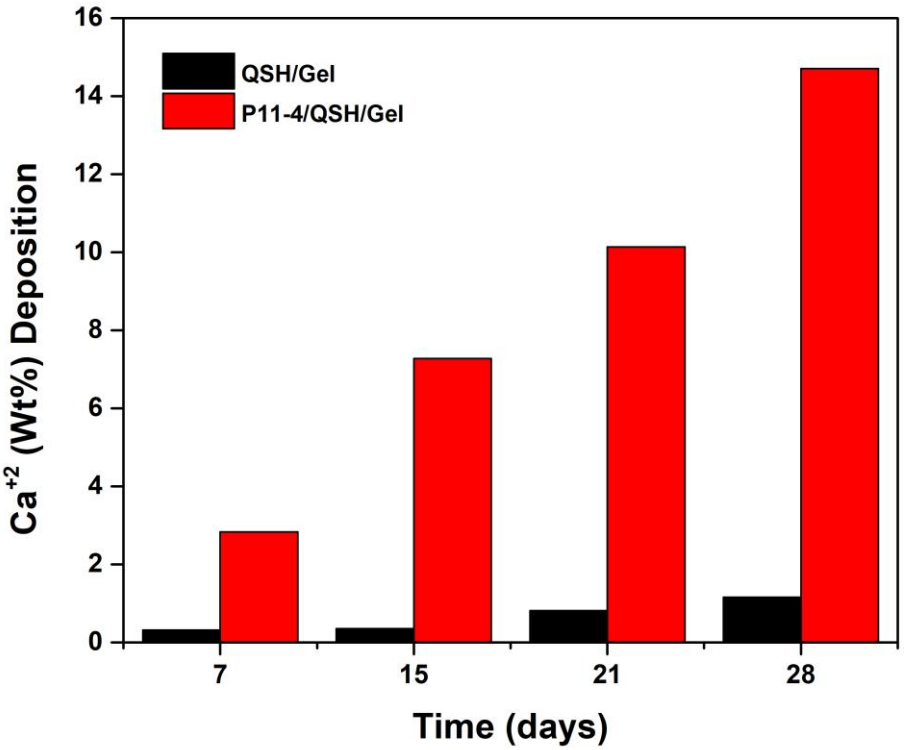

Figure 44. Ca^{+2} (Wt%) deposition of long-term cell cultured QSH/Gel and P11-4/QSH/Gel scaffolds.

CHAPTER 4

CONCLUSION

The field of dental tissue engineering deals with problems caused by caries, trauma, and erosion characterized by injury and loss of dental tissues or the entire tooth. Although many advanced biomaterials are available for tooth restoration, their use is not entirely satisfactory. In the last few decades, the role of molecular control in the process of tooth mineralization has received great attention. Biomaterial scaffolds, especially hydrogels, play a very important role in dental tissue regeneration due to their high applicability in the dental field due to their tunable properties, such as biocompatibility, biodegradability, and mineral formation. In this thesis, a new biomimetic peptide-based hydrogel bio-ink was developed and 3D bioprinted for use in dental tissue engineering. The hydrogel obtained from quince seeds has been used in regenerative medicine for decades due to its antioxidant properties without any cytotoxic effect. Quince seed hydrogel (QSH) is a biomaterial based on glucuronic acid and xylose (glucuronoxylan). Glucuronoxylan is known as a widely available and easily accessible, biocompatible, and water-soluble polysaccharide, which is highly swellable in water due to its highly hydrophilic R-groups. According to printability studies, QSH showed excellent bioprinting properties to form scaffolds suitable for cell culture studies. In addition, it can be said that the hydrogel has high protein adsorption and swelling properties and high mechanical strength. However, the cell viability results of QSH were inconsistent due to the content that can vary from batch to batch and the long adaptation time of cells. Gelatin has temperature-dependent viscosity but provides a high cell proliferation rate with similarity to native ECM. Therefore, with the synergistic effect of QSH and Gelatin, the printability of Gelatin and the cell viability of the QSH were improved. P11-4 peptide is a self-assembling and biocompatible peptide that is designed to use in dental tissue engineering studies due to its amino acid sequences. P11-4 can form a 3D hydrogel and they have a high affinity to hydroxyapatite which is obligatory to form dental tissue. The P11-4 peptide has shown potential by regenerating demineralized tooth and is designed to promote the formation of *de novo* hydroxyapatite crystals on its surface by increasing net mineral gain. It interacts with collagen type I, increases the resistance of collagen fibers to proteolysis, and improves stability. Also, the Ca^{2+}-

binding sites of the peptide surface correspond to the exact spacing of the Ca^{2+} ions in the hydroxyapatite crystal formation. P11-4 peptide was added to QSH/Gelatin as a mineralization factor. With the peptide addition, high cell viability rates and increased mineral formation were observed. Printability of P11-4/QSH/Gel bio-ink was optimized and swelling ratio, protein adsorption capacity, surface morphology, viscosity, and mechanical properties were characterized for bioprinted P11-4/QSH/Gel scaffolds. In the light of these results obtained from characterization and optimization studies; hybrid bio-ink consisting of 100 μM P11-4, 100 mg/mL QSH, and 10 mg/mL Gel with a 10:1 QSH:Gel ratio have been selected and utilized for 3D cell culture studies. The final form of the P11-4/QSH/Gel scaffold has an excellent water holding capacity, which is 21.6-fold of its own dry weight. 3D cell culture studies were performed with SaOS-2 cells, which were used as a dental model. Alizarin Red Staining was used to observe mineralized areas on the biomimetic scaffold and considerably high mineral formation was obtained for dental tissue engineering applications. In conclusion the study, results show that the findings are correlated with previous studies, and biomimetic P11-4/QSH/Gel bio-ink has great potential for dental tissue engineering applications. In addition, long-term cell culture results show that this newly developed bio-ink has high mineralization ability, and it is promising to be used in the field of dental tissue engineering.

REFERENCES

Afewerki, Samson, Amir Sheikhi, Soundarapandian Kannan, Samad Ahadian, and Ali Khademhosseini. 2019. “Gelatin-Polysaccharide Composite Scaffolds for 3D Cell Culture and Tissue Engineering: Towards Natural Therapeutics.” *Bioengineering & Translational Medicine* 4 (1): 96–115. https://doi.org/10.1002/btm2.10124.

Agents, Cross-linking. 2021. “Comparative Study of Gelatin Hydrogels Modified by Various,” 1–15.

Ahmed, Enas M. 2015. “Hydrogel: Preparation, Characterization, and Applications: A Review.” *Journal of Advanced Research* 6 (2): 105–21. https://doi.org/10.1016/J.JARE.2013.07.006.

Alkilzy, M., R. M. Santamaria, J. Schmoeckel, and C. H. Splieth. 2018a. “Treatment of Carious Lesions Using Self-Assembling Peptides.” *Https://Doi.Org/10.1177/0022034517737025* 29 (1): 42–47. https://doi.org/10.1177/0022034517737025.

———. 2018b. “Treatment of Carious Lesions Using Self-Assembling Peptides.” *Advances in Dental Research* 29 (1): 42–47. https://doi.org/10.1177/0022034517737025.

Araújo, Isaac Jordão de Souza, Gustavo Narvaes Guimarães, Renato Assis Machado, Luiz Eduardo Bertassoni, Robert Philip Wynn Davies, and Regina Maria Puppin-Rontani. 2022. “Self-Assembly Peptide P11-4 Induces Mineralization and Cell-Migration of Odontoblast-like Cells.” *Journal of Dentistry* 121 (November 2021). https://doi.org/10.1016/j.jdent.2022.104111.

Ashraf, Muhammad U., Gulzar Muhammad, Muhammad A. Hussain, and Syed N.A. Bukhari. 2016. “Cydonia Oblonga M., A Medicinal Plant Rich in Phytonutrients for Pharmaceuticals.” *Frontiers in Pharmacology* 7 (JUN): 163. https://doi.org/10.3389/FPHAR.2016.00163/BIBTEX.

Atala, Anthony. 1999. “Engineering Tissues and Organs.” *Current Opinion in Urology* 9 (6): 517–26. https://doi.org/10.1097/00042307-199911000-00005.

Bazos, Panaghiotis, DDS Emulation, Greece Pascal Magne, and Sybil Harrington Professor of Esthetic Dentistry. 2011. :":8-19) THE EUROPEAN JOURNAL OF ESTHETIC DENTISTRY VOLUME 6 • NUMBER 1 • SPRING." *THE EUROPEAN JOURNAL OF ESTHETIC DENTISTRY* 6.

Begam, Tamanna, A. K. Nagpal, and Reena Singhal. 2003. "A Comparative Study of Swelling Properties of Hydrogels Based on Poly(Acrylamide-Co-Methyl Methacrylate) Containing Physical and Chemical Crosslinks." *Journal of Applied Polymer Science* 89 (3): 779–86. https://doi.org/10.1002/APP.12270.

Bermúdez, Mercedes, Lía Hoz, Gonzalo Montoya, Mikado Nidome, Adriana Pérez-Soria, Enrique Romo, Uriel Soto-Barreras, et al. 2021. "Bioactive Synthetic Peptides for Oral Tissues Regeneration." *Frontiers in Materials* 8 (April): 63. https://doi.org/10.3389/FMATS.2021.655495/BIBTEX.

Berthiaume, François, and Martin L. Yarmush. 2003. "Tissue Engineering." *Encyclopedia of Physical Science and Technology*, January, 817–42. https://doi.org/10.1016/B0-12-227410-5/00783-3.

Bozycki, Lukasz, Magdalena Komiazyk, Saida Mebarek, Rene Buchet, Slawomir Pikula, and Agnieszka Strzelecka-Kiliszek. 2018. "Analysis of Minerals Produced by HFOB 1.19 and Saos-2 Cells Using Transmission Electron Microscopy with Energy Dispersive X-Ray Microanalysis." *Journal of Visualized Experiments* 2018 (136). https://doi.org/10.3791/57423.

Breslin, Susan, and Lorraine O'Driscoll. 2013. "Three-Dimensional Cell Culture: The Missing Link in Drug Discovery." *Drug Discovery Today* 18 (5–6): 240–49. https://doi.org/10.1016/j.drudis.2012.10.003.

Brown, P.W. 2001. "Calcium Phosphates in Biomedical Engineering." *Encyclopedia of Materials: Science and Technology*, January, 893–97. https://doi.org/10.1016/B0-08-043152-6/00170-4.

Budak, Kamil, Oguz Sogut, and Umran Aydemir Sezer. 2020. "A Review on Synthesis and Biomedical Applications of Polyglycolic Acid." *Journal of Polymer Research* 27 (8): 1–19. https://doi.org/10.1007/S10965-020-02187-1/FIGURES/8.

Cummins, D. 2013. “The Development and Validation of a New Technology, Based upon 1.5% Arginine, an Insoluble Calcium Compound and Fluoride, for Everyday Use in the Prevention and Treatment of Dental Caries.” *Journal of Dentistry* 41 (SUPPL. 2): S1–11. https://doi.org/10.1016/J.JDENT.2010.04.002.

Daffre, Sirlei, Philippe Bulet, Alberto Spisni, Laurence Ehret-Sabatier, Elaine G. Rodrigues, and Luiz R. Travassos. 2008. “Bioactive Natural Peptides.” *Studies in Natural Products Chemistry* 35 (C): 597–691. https://doi.org/10.1016/S1572-5995(08)80015-4.

Dawasaz, Ali Azhar, Rafi Ahmad Togoo, Zuliani Mahmood, Ahmad Azlina, and Kannan Thirumulu Ponnuraj. 2022a. “Effectiveness of Self-Assembling Peptide (P11-4) in Dental Hard Tissue Conditions: A Comprehensive Review.” *Polymers* 14 (4): 1–15. https://doi.org/10.3390/polym14040792.

———. 2022b. “Effectiveness of Self-Assembling Peptide (P11-4) in Dental Hard Tissue Conditions: A Comprehensive Review.” *Polymers 2022, Vol. 14, Page 792* 14 (4): 792. https://doi.org/10.3390/POLYM14040792.

Detsch, Rainer, Julia Will, Jasmin Hum, Judith A Roether, Aldo R Boccaccini, and Biocompatibility -. 2018. “Biomaterials.” *Cell Culture Technology, Learning Materials in Biosciences*, 91–105. https://doi.org/10.1007/978-3-319-74854-2_6.

Dey, Pinki. 2020. “Bone Mineralisation during Osteoporosis.” *Contemporary Topics about Phosphorus in Biology and Materials*, 1–18.

Duailibi, M. T., S. E. Duailibi, C. S. Young, J. D. Bartlett, J. P. Vacanti, and P. C. Yelick. 2004. “Bioengineered Teeth from Cultured Rat Tooth Bud Cells.” *Journal of Dental Research* 83 (7): 523–28. https://doi.org/10.1177/154405910408300703.

El-Sherbiny, Ibrahim M., and Magdi H. Yacoub. 2013. “Hydrogel Scaffolds for Tissue Engineering: Progress and Challenges.” *Global Cardiology Science and Practice* 2013 (3): 38. https://doi.org/10.5339/GCSP.2013.38/CITE/REFWORKS.

Eltom, Abdalla, Gaoyan Zhong, and Ameen Muhammad. 2019. “Scaffold Techniques and Designs in Tissue Engineering Functions and Purposes: A Review.” *Advances in Materials Science and Engineering* 2019. https://doi.org/10.1155/2019/3429527.

Fernandes, Hugo, Lorenzo Moroni, Clemens Van Blitterswijk, and Jan De Boer. 2009. "Extracellular Matrix and Tissue Engineering Applications." *Journal of Materials Chemistry* 19 (31): 5474–84. https://doi.org/10.1039/B822177D.

Flieger, M., M. Kantorová, A. Prell, T. Řezanka, and J. Votruba. 2003. "Biodegradable Plastics from Renewable Sources." *Folia Microbiologica* 48 (1): 27–44. https://doi.org/10.1007/BF02931273.

Gao, Teng, Gregory J. Gillispie, Joshua S. Copus, Anil P.R. Kumar, Young Joon Seol, Anthony Atala, James J. Yoo, and Sang Jin Lee. 2018. "Optimization of Gelatin-Alginate Composite Bioink Printability Using Rheological Parameters: A Systematic Approach." *Biofabrication* 10 (3): 034106. https://doi.org/10.1088/1758-5090/AACDC7.

Garcia-Cruz, M. R., A. Postma, J. E. Frith, and L. Meagher. 2021. "Printability and Bio-Functionality of a Shear Thinning Methacrylated Xanthan–Gelatin Composite Bioink." *Biofabrication* 13 (3): 035023. https://doi.org/10.1088/1758-5090/ABEC2D.

Ghasemiyeh, Parisa, and Soliman Mohammadi-Samani. 2019. "Hydrogels as Drug Delivery Systems; Pros and Cons." *Trends in Pharmaceutical Sciences* 5 (1): 7–24. https://doi.org/10.30476/TIPS.2019.81604.1002.

Ghumman, Shazia Akram, Arshad Mahmood, Sobia Noreen, Mavra Rana, Huma Hameed, Bushra Ijaz, Sara Hasan, Afeefa Aslam, and Muhammad Fayyaz ur Rehman. 2022. "Formulation and Evaluation of Quince Seeds Mucilage – Sodium Alginate Microspheres for Sustained Delivery of Cefixime and Its Toxicological Studies." *Arabian Journal of Chemistry* 15 (6): 103811. https://doi.org/10.1016/j.arabjc.2022.103811.

Gregory, Carl A., W. Grady Gunn, Alexandra Peister, and Darwin J. Prockop. 2004. "An Alizarin Red-Based Assay of Mineralization by Adherent Cells in Culture: Comparison with Cetylpyridinium Chloride Extraction." *Analytical Biochemistry* 329 (1): 77–84. https://doi.org/10.1016/J.AB.2004.02.002.

Habibi, Neda, Nazila Kamaly, Adnan Memic, and Hadi Shafiee. 2016. "Self-Assembled Peptide-Based Nanostructures: Smart Nanomaterials toward Targeted Drug

Delivery.” *Nano Today* 11 (1): 41–60. https://doi.org/10.1016/J.NANTOD.2016.02.004.

Haldar, Swati, Debrupa Lahiri, and Partha Roy. 2019. “3D Print Technology for Cell Culturing.” *3D Printing Technology in Nanomedicine*, January, 83–114. https://doi.org/10.1016/B978-0-12-815890-6.00005-0.

Hamauzu, Yasunori, Miho Irie, Makoto Kondo, and Tomoyuki Fujita. 2008. “Antiulcerative Properties of Crude Polyphenols and Juice of Apple, and Chinese Quince Extracts.” *Food Chemistry* 108 (2): 488–95. https://doi.org/10.1016/J.FOODCHEM.2007.10.084.

Hayashi, Mirian A.F., Frédéric Ducancel, and Katsuhiro Konno. 2012. “Natural Peptides with Potential Applications in Drug Development, Diagnosis, and/or Biotechnology.” *International Journal of Peptides* 2012. https://doi.org/10.1155/2012/757838.

Hemmati, A. A., and F. Mohammadian. 2009. “An Investigation into the Effects of Mucilage of Quince Seeds on Wound Healing in Rabbit.” *Https://Doi.Org/10.1300/J044v07n04_05* 7 (4): 41–46. https://doi.org/10.1300/J044V07N04_05.

Hoffman, Allan S. 2012. “Hydrogels for Biomedical Applications.” *Advanced Drug Delivery Reviews* 64 (SUPPL.): 18–23. https://doi.org/10.1016/J.ADDR.2012.09.010.

Horst, Britt ter, Naiem S. Moiemen, and Liam M. Grover. 2019. “Natural Polymers: Biomaterials for Skin Scaffolds.” *Biomaterials for Skin Repair and Regeneration*, January, 151–92. https://doi.org/10.1016/B978-0-08-102546-8.00006-6.

Hospodiuk, Monika, Madhuri Dey, Donna Sosnoski, and Ibrahim T. Ozbolat. 2017. “The Bioink: A Comprehensive Review on Bioprintable Materials.” *Biotechnology Advances* 35 (2): 217–39. https://doi.org/10.1016/J.BIOTECHADV.2016.12.006.

Ige, Oladeji O., Lasisi E. Umoru, and Sunday Aribo. 2012. “Natural Products: A Minefield of Biomaterials.” *ISRN Materials Science* 2012 (May): 1–20. https://doi.org/10.5402/2012/983062.

Izadyari Aghmiuni, Azadeh, Saeed Heidari Keshel, Farshid Sefat, and Azim Akbarzadeh Khiyavi. 2020. “Quince Seed Mucilage-Based Scaffold as a Smart Biological Substrate to Mimic Mechanobiological Behavior of Skin and Promote Fibroblasts Proliferation and h-ASCs Differentiation into Keratinocytes.” *International Journal of Biological Macromolecules* 142 (January): 668–79. https://doi.org/10.1016/J.IJBIOMAC.2019.10.008.

Jaipan, Panupong, Alexander Nguyen, and Roger J. Narayan. 2017. “Gelatin-Based Hydrogels for Biomedical Applications.” *MRS Communications* 7 (3): 416–26. https://doi.org/10.1557/mrc.2017.92.

Jouki, Mohammad, Seyed Ali Mortazavi, Farideh Tabatabaei Yazdi, and Arash Koocheki. 2014. “Characterization of Antioxidant-Antibacterial Quince Seed Mucilage Films Containing Thyme Essential Oil.” *Carbohydrate Polymers* 99: 537–46. https://doi.org/10.1016/J.CARBPOL.2013.08.077.

Jouki, Mohammad, Farideh Tabatabaei Yazdi, Seyed Ali Mortazavi, and Arash Koocheki. 2013. “Physical, Barrier and Antioxidant Properties of a Novel Plasticized Edible Film from Quince Seed Mucilage.” *International Journal of Biological Macromolecules* 62: 500–507. https://doi.org/10.1016/J.IJBIOMAC.2013.09.031.

Kind, L., S. Stevanovic, S. Wuttig, S. Wimberger, J. Hofer, B. Müller, and U. Pieles. 2017. “Biomimetic Remineralization of Carious Lesions by Self-Assembling Peptide.” *Https://Doi.Org/10.1177/0022034517698419* 96 (7): 790–97. https://doi.org/10.1177/0022034517698419.

Koch, Franziska, Katharina Ekat, David Kilian, Timm Hettich, Oliver Germershaus, Herrmann Lang, Kirsten Peters, and Bernd Kreikemeyer. 2019. “A Versatile Biocompatible Antibiotic Delivery System Based on Self-Assembling Peptides with Antimicrobial and Regenerative Potential.” *Advanced Healthcare Materials* 8 (13): 1900167. https://doi.org/10.1002/ADHM.201900167.

Koch, Franziska, Nina Meyer, Silvio Valdec, Ronald E. Jung, and Stephanie H. Mathes. 2020. “Development and Application of a 3D Periodontal in Vitro Model for the Evaluation of Fibrillar Biomaterials.” *BMC Oral Health* 20 (1): 1–12.

https://doi.org/10.1186/s12903-020-01124-4.

Koutsopoulos, Sotirios. 2016. “Self-Assembling Peptide Nanofiber Hydrogels in Tissue Engineering and Regenerative Medicine: Progress, Design Guidelines, and Applications.” *Journal of Biomedical Materials Research - Part A* 104 (4): 1002–16. https://doi.org/10.1002/jbm.a.35638.

Labet, Marianne, and Wim Thielemans. 2009. “Synthesis of Polycaprolactone: A Review.” *Chemical Society Reviews* 38 (12): 3484–3504. https://doi.org/10.1039/B820162P.

Langhans, Sigrid A. 2018. “Three-Dimensional in Vitro Cell Culture Models in Drug Discovery and Drug Repositioning.” *Frontiers in Pharmacology* 9 (JAN): 6. https://doi.org/10.3389/FPHAR.2018.00006/BIBTEX.

Manavitehrani, Iman, Ali Fathi, Hesham Badr, Sean Daly, Ali Negahi Shirazi, and Fariba Dehghani. 2016. “Biomedical Applications of Biodegradable Polyesters.” *Polymers* 8 (1). https://doi.org/10.3390/polym8010020.

Manna, Sara La, Concetta Di Natale, Daniele Florio, and Daniela Marasco. 2018. “Peptides as Therapeutic Agents for Inflammatory-Related Diseases.” *International Journal of Molecular Sciences 2018, Vol. 19, Page 2714* 19 (9): 2714. https://doi.org/10.3390/IJMS19092714.

Manna, Sara La, Concetta Di Natale, Valentina Onesto, and Daniela Marasco. 2021. “Self-Assembling Peptides: From Design to Biomedical Applications.” *International Journal of Molecular Sciences* 22 (23): 12662. https://doi.org/10.3390/IJMS222312662.

Milojević, Marko, Gregor Harih, Boštjan Vihar, Jernej Vajda, Lidija Gradišnik, Tanja Zidarič, Karin Stana Kleinschek, Uroš Maver, and Tina Maver. 2021. “Hybrid 3D Printing of Advanced Hydrogel-Based Wound Dressings with Tailorable Properties.” *Pharmaceutics* 13 (4). https://doi.org/10.3390/PHARMACEUTICS13040564.

Murai, Kazuki, Yosuke Funamizu, Toshihiko Ogura, and Keishi Nishio. 2021. “Bioinspired Mineralization of Calcium Carbonate in Peptide Hydrogel Acting as a

Multifunctional Three-Dimensional Template." *Https://Doi.Org/10.1080/21870764.2021.1911060*. https://doi.org/10.1080/21870764.2021.1911060.

Murphy, Sean V, and Anthony Atala. 2014. "3D Bioprinting of Tissues and Organs." *Nature Publishing Group*. https://doi.org/10.1038/nbt.2958.

Muttenthaler, Markus, Glenn F. King, David J. Adams, and Paul F. Alewood. 2021. "Trends in Peptide Drug Discovery." *Nature Reviews. Drug Discovery* 20 (4): 309–25. https://doi.org/10.1038/S41573-020-00135-8.

Natale, Concetta Di, Sara La Manna, Ilaria De Benedictis, Paola Brandi, and Daniela Marasco. 2020. "Perspectives in Peptide-Based Vaccination Strategies for Syndrome Coronavirus 2 Pandemic." *Frontiers in Pharmacology* 11 (December): 1779. https://doi.org/10.3389/FPHAR.2020.578382/BIBTEX.

Nikolova, Maria P., and Murthy S. Chavali. 2019. "Recent Advances in Biomaterials for 3D Scaffolds: A Review." *Bioactive Materials* 4 (December): 271–92. https://doi.org/10.1016/J.BIOACTMAT.2019.10.005.

Ouyang, Liliang, Christopher B. Highley, Christopher B. Rodell, Wei Sun, and Jason A. Burdick. 2016. "3D Printing of Shear-Thinning Hyaluronic Acid Hydrogels with Secondary Cross-Linking." *ACS Biomaterials Science and Engineering* 2 (10): 1743–51. https://doi.org/10.1021/ACSBIOMATERIALS.6B00158/SUPPL_FILE/AB6B00158_SI_001.PDF.

Ouyang, Liliang, Rui Yao, Yu Zhao, and Wei Sun. 2016. "Effect of Bioink Properties on Printability and Cell Viability for 3D Bioplotting of Embryonic Stem Cells." *Biofabrication* 8 (3): 035020. https://doi.org/10.1088/1758-5090/8/3/035020.

Özmen, Ece, Özüm Yıldırım, and Ahu Arslan-Yıldız. 2023. "Bioprinting of Hydrogels for Tissue Engineering and Drug Screening Applications." *Advances in Biomedical Polymers and Composites*, January, 183–221. https://doi.org/10.1016/B978-0-323-88524-9.00028-0.

Raeburn, Jaclyn, Andre Zamith Cardoso, and Dave J. Adams. 2013. "The Importance of

the Self-Assembly Process to Control Mechanical Properties of Low Molecular Weight Hydrogels." *Chemical Society Reviews* 42 (12): 5143–56. https://doi.org/10.1039/c3cs60030k.

Rahali, Kamel, Ghazi Ben Messaoud, Cyril J.F. Kahn, Laura Sanchez-Gonzalez, Mouna Kaci, Franck Cleymand, Solenne Fleutot, Michel Linder, Stéphane Desobry, and Elmira Arab-Tehrany. 2017. "Synthesis and Characterization of Nanofunctionalized Gelatin Methacrylate Hydrogels." *International Journal of Molecular Sciences* 18 (12). https://doi.org/10.3390/ijms18122675.

Rani, Grandhe U., and Suraj Sharma. 2021. "Biopolymers, Bioplastics and Biodegradability: An Introduction." *Reference Module in Materials Science and Materials Engineering*, January. https://doi.org/10.1016/B978-0-12-820352-1.00131-0.

Rios, Hector F., Zhao Lin, BiNa Oh, Chan Ho Park, and William V. Giannobile. 2011. "Cell- and Gene-Based Therapeutic Strategies for Periodontal Regenerative Medicine." *Journal of Periodontology* 82 (9): 1223. https://doi.org/10.1902/JOP.2011.100710.

Roseti, Livia, Valentina Parisi, Mauro Petretta, Carola Cavallo, Giovanna Desando, Isabella Bartolotti, and Brunella Grigolo. 2017. "Scaffolds for Bone Tissue Engineering: State of the Art and New Perspectives." *Materials Science and Engineering: C* 78 (September): 1246–62. https://doi.org/10.1016/J.MSEC.2017.05.017.

Schmidt, Christine E., and Jennie M. Baier. 2000. "Acellular Vascular Tissues: Natural Biomaterials for Tissue Repair and Tissue Engineering." *Biomaterials* 21 (22): 2215–31. https://doi.org/10.1016/S0142-9612(00)00148-4.

Sedlakova Kondelova, Paulina, Alaa Mannaa, Claudine Bommer, Marwa Abdelaziz, Laurent Daeniker, Enrico di Bella, and Ivo Krejci. 2020. "Efficacy of P11-4 for the Treatment of Initial Buccal Caries: A Randomized Clinical Trial." *Scientific Reports 2020 10:1* 10 (1): 1–9. https://doi.org/10.1038/s41598-020-77057-3.

Shrivastava, Anshuman. 2018. "Introduction to Plastics Engineering." *Introduction to Plastics Engineering*, January, 1–16. https://doi.org/10.1016/B978-0-323-39500-

7.00001-0.

Sohail Zafar, Muhammad, Faiza Amin, Muhmmad Amber Fareed, Hani Ghabbani, Samiya Riaz, Zohaib Khurshid, and Naresh Kumar. n.d. “Biomimetics Biomimetic Aspects of Restorative Dentistry Biomaterials.” Accessed August 20, 2022. https://doi.org/10.3390/biomimetics5030034.

Soltan, Nikoo, Liqun Ning, Fatemeh Mohabatpour, Petros Papagerakis, and Xiongbiao Chen. 2019. “Printability and Cell Viability in Bioprinting Alginate Dialdehyde-Gelatin Scaffolds.” *ACS Biomaterials Science and Engineering* 5 (6): 2976–87. https://doi.org/10.1021/acsbiomaterials.9b00167.

Sousa, J. P. de, R. G. Carvalho, L. F. Barbosa-Martins, R. J.S. Torquato, K. C.U. Mugnol, F. D. Nascimento, I. L.S. Tersariol, and R. M. Puppin-Rontani. 2019. “The Self-Assembling Peptide P11-4 Prevents Collagen Proteolysis in Dentin.” *Https://Doi.Org/10.1177/0022034518817351* 98 (3): 347–54. https://doi.org/10.1177/0022034518817351.

Tappa, Karthik, and Udayabhanu Jammalamadaka. 2018. “Novel Biomaterials Used in Medical 3D Printing Techniques.” *Journal of Functional Biomaterials* 9 (1). https://doi.org/10.3390/JFB9010017.

Tibbitt, Mark W., and Kristi S. Anseth. 2009. “Hydrogels as Extracellular Matrix Mimics for 3D Cell Culture.” *Biotechnology and Bioengineering* 103 (4): 655–63. https://doi.org/10.1002/BIT.22361.

Versluis, Frank, Jan H. van Esch, and Rienk Eelkema. 2016. “Synthetic Self-Assembled Materials in Biological Environments.” *Advanced Materials* 28 (23): 4576–92. https://doi.org/10.1002/adma.201505025.

Wu, Xinchen, Kierra Walsh, Brianna L. Hoff, and Gulden Camci-Unal. 2020. “Mineralization of Biomaterials for Bone Tissue Engineering.” *Bioengineering* 7 (4): 1–24. https://doi.org/10.3390/bioengineering7040132.

Yildirim, Özüm, and Ahu Arslan-Yildiz. 2022. “Development of a Hydrocolloid Bio-Ink for 3D Bioprinting.” *Biomaterials Science*. https://doi.org/10.1039/D2BM01184K.

Young, C. S., S. Terada, J. P. Vacanti, M. Honda, J. D. Bartlett, and P. C. Yelick. 2002. "Tissue Engineering of Complex Tooth Structures on Biodegradable Polymer Scaffolds." *Journal of Dental Research* 81 (10): 695–700. https://doi.org/10.1177/154405910208101008.

Yue, Beatrice. 2014. "Biology of the Extracellular Matrix: An Overview." *Journal of Glaucoma* 23 (8): S20. https://doi.org/10.1097/IJG.0000000000000108.

Zhang, Shuguang. 2017. "Discovery and Design of Self-Assembling Peptides." *Interface Focus* 7 (6). https://doi.org/10.1098/RSFS.2017.0028.

Zhu, Junmin. 2010. "Bioactive Modification of Poly(Ethylene Glycol) Hydrogels for Tissue Engineering." *Biomaterials* 31 (17): 4639–56. https://doi.org/10.1016/J.BIOMATERIALS.2010.02.044.